

Sensitivity Analysis and Performance Prediction Methodology for MEMS
Design

by

Faik Can Meral

A Thesis Submitted to the
Graduate School of Engineering
in Partial Fulfillment of the Requirements for
the Degree of

Master of Science

in

Mechanical Engineering

Koç University

August, 2005

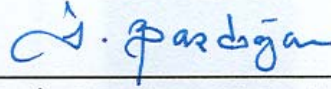
Koc University
Graduate School of Sciences and Engineering

This is to certify that I have examined this copy of a master's thesis by

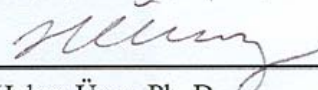
Faik Can Meral

and have found that it is complete and satisfactory in all respects,
and that any and all revisions required by the final
examining committee have been made.

Committee Members:



İpek Başdoğan, Ph. D. (Advisor)



Hakan Ürey, Ph. D.



Erdem Alaca, Ph. D.

Date:

9 / 8 / 2005

ABSTRACT

Future optical micro systems such as Micro Electro Mechanical Systems (MEMS) scanners and micro-mirrors will extend the resolution and sensitivity offered by their predecessors. These systems face the challenge of achieving nanometer precision subjected to various disturbances. Predicting the performance of such systems early in the design process can significantly impact the design cost and also improve the quality of the design. Our approach aims to predict the performance of such systems under various disturbance sources and develop a generalized design approach for MEMS structures including a sensitivity analysis framework. In this study, we use ANSYS for modeling and analysis of a torsional MEMS scanner mirror. ANSYS modal analysis results, which are eigenvalues (natural frequencies) and eigenvectors (mode shapes), are used to obtain the state space representation of the mirror. The state space model of the scanner mirror is reduced using various reduction techniques to eliminate the states that are insignificant for the transfer functions of interest. The results of these techniques are compared to obtain the best approach for achieving a lower order model that still contains all of the relevant dynamics of the original model. After the model size is reduced significantly, a disturbance analysis is performed using Lyapunov approach to obtain root-mean-square (RMS) values of the mirror rotation angle under the effect of a disturbance torque. The Lyapunov approach results were validated using a time domain analysis. The sensitivity framework described in this study is directly related to the disturbance analysis framework. Analytical formulas are derived for the calculation of the modal parameter sensitivities and the results are verified by the finite difference method. The analytical formulas for the calculation of physical parameter sensitivities are described but they are found to be very inefficient due to the complexity and computational expense in calculating the eigenvalue and eigenvector derivatives included in these equations. Instead, the finite difference method is used to calculate the physical parameter sensitivities for the torsional MEMS scanner. Disturbance characteristics of the microscanners are measured, using the experimental techniques. The resulting data is utilized in the disturbance analysis framework.

ÖZET

Geleceğin, mikro-elektro-mekanik sistem tarayıcıları ve mikro aynalar gibi optik mikro sistemleri öncülleri tarafından sunulan çözünürlüğü ve hassasiyeti geçeceklerdir. Bu sistemler mekanik ya da elektronik bozucu etmenlerin yoğun olduğu ortamlarda dahi nanometre ölçüsünde toleransları yakalamalıdır. Sistem performansını erken tasarım aşamasında saptamak tasarım masrafını düşürürken, dizayn kalitesini önemli ölçüde geliştirecektir. Yaklaşımımız, bu sistemlerin bozucu etmenler karşısında sergilediği performansını öngören ve hassasiyet analizini (sensitivity analysis) de kapsayan bir dizayn aracı geliştirmeyi amaçlamaktadır. ANSYS modal analiz sonuçları olan doğal frekans ve mod şekilleri, aynanın durum-yer (state-space) gösterimini elde etmek için kullanılmaktadır. Tarayıcı aynanın durum-yer modeli transfer fonksiyonları için önemsiz sayılabilecek durumları elemek için çeşitli indirgeme teknikleri kullanarak sadeleştirilebilir. Bu tekniklerin sonuçları, orijinal modelin bütün ilgili dinamiklerini kapsayacak; daha düşük derece bir model elde etmek için karşılaştırılabilir. Model, önemli ölçüde indirgindikten sonra, bozucu tork etkisi altında aynanın dönme açısının standart sapması (RMS) Lyapunov yaklaşımı kullanılarak hesaplanmıştır. Bu çalışmada konu edilen hassasiyet analizi çerçevesi, doğrudan bozunma analizi çerçevesine bağlıdır. Modal parametre hassasiyetlerinin hesaplanması için analitik formüller oluşturulup, sonuçlar sonlu farklılıklar metodu kullanılarak doğrulanabilir. Fiziksel parametre hassasiyetlerini hesaplamak için geliştirilen analitik formüller de çalışma dahilinde açıklanmıştır, fakat formüller karmaşıklıkları ve içerdikleri doğal frekans ve mod şekli türevlerinin hesaplamasının zorluğu yüzünden oldukça verimsiz bulunmuşlardır. Onun yerine, burulmalı MEMS tarayıcısı için fiziksel parametre hassasiyetlerini hesaplamak için sonlu farklılıklar metodu kullanılmıştır.

ACKNOWLEDGEMENTS

I would like to express my sincere gratitude to my thesis advisor Dr. İpek Başdoğan for giving me the opportunity to carry out this thesis within her research team. I appreciate Koc University College of Engineering for supporting me through travel grants that enabled me to participate international conferences.

I also would like to thank to Dr. Hakan Ürey and Dr. Erdem Alaca for taking part in my thesis jury. Additional thanks to Dr. Ürey for his hours spent to discuss my results and for his invaluable advices.

As my colleagues, many thanks to Evren, Burak, Hüseyin, Ufuk, Göker, Sabri Bora, and Volkan for making those long hours spent in the office as enjoyable as they were. The OML staff Çağlar, Olgaç, Hamdi and Özgür for their hospitality... To Ozan for his patience in revising and decoding my code... Of course, my appreciations and gratitude go to Davut Otar for his incredible friendship from day and night and even though from Afghanistan.

Finally, I would like to thank to Ekrem Bey, Meral Hanım and Başak. Even though you were not here with me, none of these would be possible without you.

LIST OF FIGURES

Figure 1.2-1: (a)Retinal Scanning Display Technology of Microvision, Inc uses a 2D MEMS microscanner. (Photo courtesy of Microvision, Inc), (b)Hand-held barcode readers are potential applications of MEMS microscanners (Photo courtesy of STAR-System, Inc).....	2
Figure 1.2-2: A microscanner for optical switching applications, shown alone and in an array.....	3
Figure 1.2-3: Torsional MEMS Scanner showing the design parameters	4
Figure 2.2-1: Finite element model of the MEMS torsional scanner. The model is created in ANSYS using 3D solid elements.....	6
Figure 2.2-2: Five fundamental vibration modes of a box shaped microscanner.....	9
Figure 2.2-3: Simplified finite element model of the MEMS torsional scanner. Beam and shell elements are used for model simplification.....	10
Figure 2.4-1: dc gain values plotted for each mode, the first mode being the torsional mode has the greatest dc gain among all	15
Figure 2.4-2: First six modes are used to construct the reduced model	17
Figure 2.4-3: Modes are sorted according to the “dc gain” and “peak gain” approach. First six modes with higher gains are used to construct the reduced model.....	17
Figure 3.2-1: Disturbance shaping filter connected in series with the mirror model	19
Figure 3.2-2: The frequency response and phase diagrams for the disturbance filter. The magnitude falls down quickly after the corner frequency (2510rad/sec ~400Hz)	20

Figure 3.2-3: Comparison of Different Corner Frequencies For Disturbance Filter	20
Figure 3.3-1: Lumped mass-spring-damper model	23
Figure 3.3-2: Time history of the disturbances. A randomly generated number array then scaled down to the expected disturbances' magnitude level	24
Figure 3.3-3: The angular displacement as a function of time. The equation of motion representing the lumped system is integrated using the MATLAB function 'lsim'. The torque input is a randomly created disturbance array	25
Figure 4.1-1: Torsional MEMS Scanner showing the design parameters	27
Figure 4.2-1: (a) The transfer function plot for the torsional scanner. Three modes can be observed while the others cannot. (b) The modes' dc gain values, however modes are sorted with respect to their dc gain contribution. Three modes having larger gains can be easily noticed among the others.....	34
Figure 4.2-2: Variation of the error between finite difference method solutions and the exact solution with respect to the perturbation factor. The error of the finite difference method grows logarithmically with the increasing perturbation size	35
Figure 4.2-3: Comparison of two different sensitivity analysis methods, applied on a cantilever beam. The physical parameters, which sensitivities are calculated with respect to are 'A' beam cross sectional area, 'E' elastic modulus, and ' ρ ' the density of the beam material	40
Figure 4.3-1: The schematic of the design procedure with performance prediction and sensitivity analysis.....	42
Figure 5.2-1: The LABView screen shot. The program is constructed in order to measure the disturbances.....	44

Figure 5.2-2: Microvision Biaxial MEMS scanner. First picture showing the scanner in the casing with the permanent magnets, below this picture coils used to drive the scanner can be seen on the outer frame. The third one is a close up picture, slow scan and fast scan frames and flexures can be identified 45

Figure 5.2-3: the schematic showing the setup for piezoresistive sensor readings. The sensors can be directly connected to an oscilloscope or a pc with a data acquisition system..... 46

Figure 5.2-4: LDV measurement point, for the torsional mode of the outer frame 47

Figure 5.2-5: Schematic view of the LDV measurement setup, for the description of “small angle θ ” assumption..... 48

Figure5.3-1: Schematic of disturbance measurement procedure..... 49

Figure 5.4-1: LDV Readings versus Piezo Sensor readings. (The noise on the piezo sensor data can be seen easily) 50

Figure 5.4-2: The position obtained by integration of the velocity and obtained from piezoresistive sensors. The left hand side y- axis represents the integrated LDV results for position, while the right hand side represents piezoresistive sensor outputs 51

Figure 5.4-3: Ideal and measured position data. The measured data seems to fit with the ideal one, however there occurs a little difference which is enough for disturbance calculations..... 52

Figure 5.4-4: The time history for the disturbances, the difference between the measured and the ideal. RMS values for the measured disturbance is calculated as 3.6×10^{-5} 52

LIST OF TABLES

Table 3.3-1: Effective mass moment of inertia and effective stiffness terms for the torsional mode of a torsional scanner	24
Table 3.3-2: Mass and mass moment of inertia terms for a rectangular mirror geometry	25
Table 3.3-3: Comparison of Lypunov approach and time domain analysis	26
Table 4.2-1: Modal parameter sensitivity analysis results of Torsional scanner. Analytic solution and finite difference solution techniques are compared	33
Table 4.2-2: Physical parameter sensitivity analysis of the torsional MEMS scanner...	41

TABLE OF CONTENTS

Chapter 1	1
INTRODUCTION	1
1.1 Generalized Design Approach.....	1
Chapter 2	6
MODELING	6
2.1 Introduction.....	6
2.2 Finite Element Model.....	6
<i>Natural Frequency and Mode Shapes</i>	7
2.3 State-Space Modeling.....	10
2.4 Model Reduction.....	13
Chapter 3	18
DISTURBANCE ANALYSIS FRAMEWORK	18
3.1 Introduction.....	18
3.2 Disturbance Analysis using Lyapunov Approach.....	18
3.3 Disturbance Analysis in Time Domain.....	23
Chapter 4	27
SENSITIVITY ANALYSIS FRAMEWORK	27
4.1 Introduction.....	27
4.2 Sensitivity Analysis Framework.....	28
4.2.1 Lagrange Multiplier Method.....	29
4.2.2 Modal Parameter Sensitivities Using Analytical Approach.....	31
4.2.3 Modal Parameter Sensitivities Using Finite Difference Approach.....	34
4.2.4 Physical Parameter Sensitivities Using Analytical Approach.....	35
4.2.5 A Benchmark Example for Physical Parameter Sensitivities Using Analytical Solution: Cantilever Beam Example.....	38
4.2.6 Physical Parameter Sensitivities Using Finite Difference Approach.....	39
4.2.7 Sensitivity Analysis of a Microscanner.....	40
4.3 Design Procedure.....	41

Chapter 5.....	43
EXPERIMENTAL STUDY.....	43
5.1 Introduction	43
5.2 Equipment	43
5.2.1 Microscanner	44
5.2.2 Piezoresistive Sensors	45
5.2.3 Laser Doppler Vibrometer.....	47
5.3 Procedure.....	48
5.4 Results	49
5.4.1 Piezoresistive Sensors and Position Measurements	49
5.4.2 LDV and Velocity Measurements	50
5.4.3 Torque Intensity	53

Chapter 1

INTRODUCTION

1.1 Generalized Design Approach

The Microsystems design and manufacturing technology is developing rapidly. There is a variety of specialized computer aided design tools in the MEMS and MOEMS area such as SUGAR [1], ANSYS [2] and FEMLAB [3]. Although these tools can provide a lot of insight into the design of MEMS devices, they are limited with the built-in algorithms. These algorithms are not expandable if the user wants to do further analysis. For conceptual design, there are a few existing design synthesis studies. Li and Antonsson [4] developed an approach for automatic synthesis of MEMS mask layouts. Mukherjee and Fedder [5] have presented a structured design method for MEMS. Other examples include the automated design synthesis method for MEMS by Zhan and et al. [6]

Our approach aims to integrate some of the existing analysis tools and develop a generalized design approach for MEMS structures. The methodologies developed in this thesis incorporate tools for analyzing end-to-end system performance and sensitivity of design parameters of MEMS devices.

The contributions of this thesis can be summarized in four areas:

- A generic MATLAB code was developed to generate the state space representation of a structure, based on the Finite Element Analysis (FEA) results. (e.g.: MEMS scanner)
- A disturbance analysis tool was developed to predict the performance of MEMS devices under the effect of various disturbance sources.
- A sensitivity analysis tool was developed to calculate the sensitivities of the design parameters for MEMS devices.
- Various experimental techniques were adopted to characterize the disturbances acting on the MEMS devices.

A microscanner mirror is chosen as the case study to demonstrate the capability of the design tools that we developed. A microscanner is a tiny movable mirror that can steer a laser beam in 1D, 2D or 3D. Due to their promising mechanical, optical and electrical properties, there has been a significant amount of research and development efforts on microscanner and micromirror

technologies. Some of the major application areas of micromirror and microscanner technologies are given below.

Display and Imaging: The fundamental application field of MEMS microscanners is the display and imaging systems [7]. Fast scanning speeds and high scan angles achieved by the microscanner technologies make them a good candidate for this type of applications. There are a wide variety of display applications that utilize MEMS devices as mirrors and scanners. Some of the display product examples are Retinal Scanning Display (RSD) and barcode readers (Figure 1.2-1).

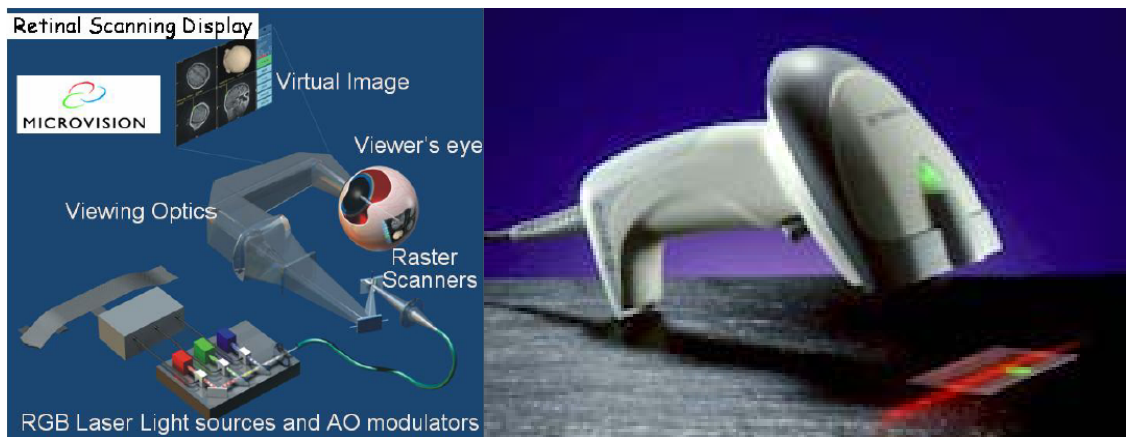


Figure 1.2-1: (a) Retinal Scanning Display Technology of Microvision, Inc uses a 2D MEMS microscanner. (Photo courtesy of Microvision, Inc)

(b) Hand-held barcode readers are potential applications of MEMS microscanners (Photo courtesy of STAR-System, Inc)

RSD is a head mounted micro-display developed by Microvision, Inc. Performance constraints for a microscanner based high-resolution display system like RSD require a very careful design of the microscanner. The trade-offs and critical issues of microscanner design for display systems are challenging, and have been the subject of several articles [8]. Barcode reading is the most important imaging application of today's microscanner technologies [9]. They offer effective solutions for reading both regular 1D and new 2D barcodes. One major issue about barcode scanners may be the mechanical reliability, since a hand-held device may experience high shocks due to dropping, hitting, etc. In addition to the mentioned devices, there are various other technologies that use microscanners for display and imaging applications [10].

Optical Switching: Another major application field of optical MEMS is the telecommunications industry [11]. Figure 1.2-2 shows a stand alone microscanner designed for optical switching; and an array of these.

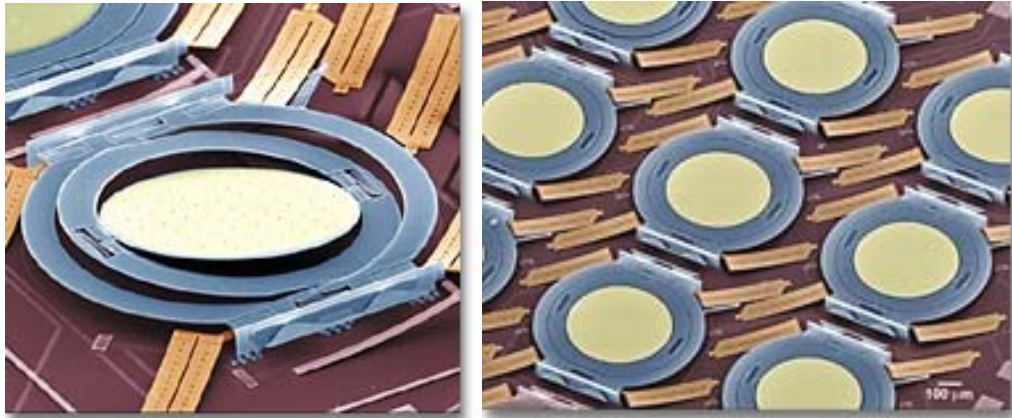


Figure 1.2-2: A microscanner for optical switching applications, shown alone and in an array.

Another application field of MEMS microscanners is spectroscopy [20]. A diffraction grating is formed on the mirror surface. As the scanner rotates, different wavelengths are diffracted onto a single photodetector, producing the spectrum of the incoming light at the detector output. Some other crucial applications of MEMS microscanners and micromirrors that were not mentioned here include endoscopic optical coherence tomography, optical storage, adaptive optics, and interferometry.

The scanning capability of such mirrors can be significantly impacted by the disturbances coming from the outside sources. Driving electronics jitter, control loop sensor errors and thermal changes in the environment are examples of disturbances that may effect the performance of the mirror during the operation mode. Accurate representation of these disturbances is important in order to predict the performance of these mirrors.

In this study, we developed a generalized design approach for MEMS devices that incorporates modeling and analysis tools in MATLAB environment. Our integrated design approach starts with the generation of Finite Element Model (FEM) of the torsional scanner mirror using ANSYS software. The details of this model are given in chapter 2. The state space

representation of the system is constructed in MATLAB using ANSYS results. The state space model is reduced using some reduction techniques which will be outlined also in chapter 2. The reduction algorithms are carefully chosen to keep the significant states for the transfer functions of interest. The input to our model is the disturbance torque acting on the mirror about the scanning axis. The output or equivalently the performance is defined as the variation of the mirror position under the effect of a disturbance torque. The absolute value of this rotation should be kept as small as possible in order to improve the performance of the mirror.

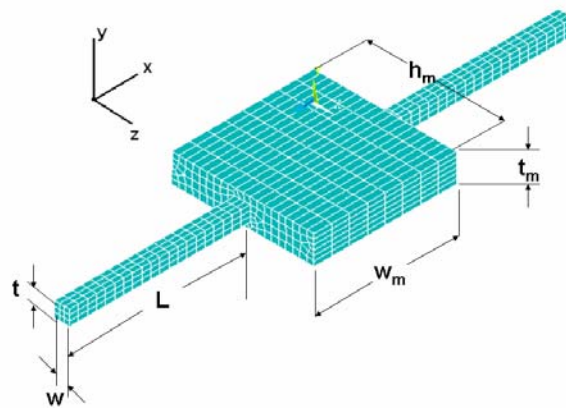


Figure 1.2-3: Torsional MEMS Scanner showing the design parameters

After developing a reduced model of the system, the next step is to predict the system performance under anticipated disturbance conditions. Chapter 3 outlines the disturbance analysis framework. A disturbance filter is generated based on the results of the experimental measurements of the disturbances on microscanners. Integrating the disturbance filter with the plant model forms the required governing equations for the overall system. The disturbance analysis is conducted using the Lyapunov approach. Lyapunov approach predicts the variation of the mirror rotation in a very accurate and efficient way. Lyapunov approach results are validated using a time domain analysis.

After determining the performance of these systems under the effect of the anticipated disturbances, the next goal is to combine the disturbance analysis with the sensitivity analysis framework. Sensitivity analysis is one of the design techniques that can be used to identify the critical design parameters for optimizing the performance of a system. Sensitivity information

provides the performance change of a system with respect to the changing design parameters. In a previous work by Shi, Ramesh and Mukherjee [13], sensitivity analysis was carried out using the direct differentiation approach to compute the design sensitivity coefficients. The coupled electromechanical design sensitivities were presented by Allen, Raulli, Maute and Frangopol [14] for a reliability based analysis. Additionally Sigmund [15] presented the use of sensitivity analysis for topological optimization of electromechanical systems.

In chapter 4, the exact modal parameter sensitivities are calculated and compared with the sensitivities calculated using the finite difference approach. While these sensitivities do identify which modes are the most important, they do not reveal directly what physical characteristics of the design should be modified to affect the modes and improve the design. Physical parameter sensitivities are more intuitive, and this fact motivates to investigate the physical parameter sensitivities for the torsional MEMS scanner. This chapter also describes the analytical formulations for the physical parameter sensitivities derived by Gutierrez [16]. But it is found to be an inefficient method for the mirror application due to the complexity and computational expense in calculating the eigenvalue and eigenvector derivatives included in these equations. Chapter 4, also summarizes the physical sensitivity analysis results obtained by using the finite difference method.

The disturbance analysis tools in Chapter 3 provide acceptable results if and only if the disturbances are modeled properly. Chapter 5, describes the experimental set-up and the techniques that we developed to characterize the disturbances.

Chapter 2 MODELING

2.1 Introduction

Finite Element Model (FEM) and Finite Element Analysis (FEA) are the most commonly used design tools for modeling and analysis. FEA provide various engineering analysis tools for many disciplines. Some of these disciplines include structural mechanics, thermodynamics, electrostatics and electromagnetism. In this chapter, we are going to use the structural modeling and modal analysis tools of the ANSYS software. The details of the structural model are given in Section 2.2. The generation of the state space model and the model reduction techniques are described in sections 2.3 and 2.4.

2.2 Finite Element Model

The finite element model of the torsional scanner mirror is created in ANSYS. The model is constructed using APDL, which stands for ANSYS Parametric Design Language. APDL provides an easy way to change the design parameters. In the first model, 3D solid elements are used and modal analysis is conducted with the model.

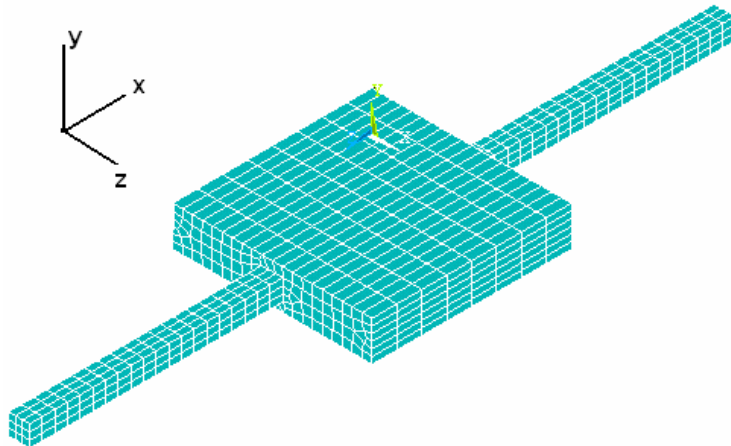


Figure 2.2-1. Finite element model of the MEMS torsional scanner. The model is created in ANSYS using 3D solid elements.

Natural Frequency and Mode Shapes

The governing equations for the undamped free vibration of multi-degree of freedom system generated by Finite Element Analysis is [17]

$$\mathbf{M}\ddot{\mathbf{z}} + \mathbf{K}\mathbf{z} = 0 \quad (2.1)$$

and a solution of the form is assumed

$$\mathbf{z} = \mathbf{\Phi} \sin(\omega t + \phi) \quad (2.2)$$

where ' $\mathbf{\Phi}$ ' is the vector of amplitudes of vibration, ' ω ' is the frequency, and ' ϕ ' is the phase angle. ' \mathbf{z} ' is the vector of physical coordinates. Differentiation of Eq. 2.2 twice with respect to time leads to

$$\ddot{\mathbf{z}} = -\omega^2 \mathbf{\Phi} \sin(\omega t + \phi) \quad (2.3)$$

substituting Eqs 2.2 and 2.3 into Eq. 2.1 lead to

$$-\omega^2 \mathbf{M}\mathbf{\Phi} \sin(\omega t + \phi) + \mathbf{K}\mathbf{\Phi} \sin(\omega t + \phi) = 0 \quad (2.4)$$

which leads to

$$\mathbf{K}\mathbf{\Phi} - \omega^2 \mathbf{M}\mathbf{\Phi} = 0 \quad (2.5)$$

Equation 2.5 which is called the standard eigenvalue problem can be considered as a system of homogenous equations in the vector of unknown amplitudes $\mathbf{\Phi}$. This equation can be written in the following form

$$[\mathbf{K} - \omega^2 \mathbf{M}]\mathbf{\Phi} = 0 \quad (2.6)$$

This equation has a nontrivial solution if and only if the coefficient matrix is singular, that is

$$|\mathbf{K} - \omega^2 \mathbf{M}| = 0 \quad (2.7)$$

This equation is called the characteristic equation and leads to a polynomial of order n in ω^2 . the roots of this polynomial denoted as $\omega_1^2, \omega_2^2, \dots, \omega_n^2$, are called the eigenvalues. The square roots of these numbers $\omega_1, \omega_2, \dots, \omega_n$, are called the natural frequencies of the undamped multi-degree of freedom system. Thus a system with n degrees of freedom has n natural frequencies.

Associated with each characteristic value ω_i there is an n -dimensional vector called the eigenvector $\mathbf{\Phi}_i$ which can be obtained by using Eq. 2.6

$$[\mathbf{K} - \omega_i^2 \mathbf{M}]\mathbf{\Phi}_i = 0 \quad (2.8)$$

This is a system of homogenous algebraic equation with a singular coefficient matrix since ω_i^2 is one of the roots of the polynomial resulting from Eq. 2.7. Therefore Eqn. 2.8 has a non-trivial

solution which defines the eigenvector Φ_i to within an arbitrary constant. The eigenvector (amplitude) Φ_i is sometimes referred to as i^{th} mode shape of vibration.

$$\Phi^T \mathbf{M} \Phi \ddot{\mathbf{x}} + \Phi^T \mathbf{C} \Phi \dot{\mathbf{x}} + \Phi^T \mathbf{K} \Phi \mathbf{x} = \mathbf{0} \quad (2.9)$$

where ' Φ ' is the combination of the eigenvectors calculated for all eigenvalues and ' \mathbf{x} ' is the vector of modal coordinates.

For the damped case equation of motion turns into

$$\mathbf{M}_p \ddot{\mathbf{x}} + \mathbf{C}_p \dot{\mathbf{x}} + \mathbf{K}_p \mathbf{x} = \mathbf{0} \quad (2.10)$$

where $\mathbf{M}_p, \mathbf{C}_p, \mathbf{K}_p$ are diagonal modal mass, damping and stiffness matrices, respectively.

Equation 2.10 can then be rewritten as ' n ' uncoupled differential equation

$$\ddot{x}_i + 2\zeta_i \omega_i \dot{x}_i + \omega_i^2 x_i = 0 \quad (2.11)$$

Where ζ_i is the modal damping factor, ω_i is the natural frequency of mode i , and n is the number of independent dof. The modal damping factor ζ_i is assumed to be 0.2%.

Natural Modes of Vibration of the Microscanner

Basic one-axis torsional scanner geometry and the first five fundamental vibration modes are illustrated in Figure 2.2-2. The figure presents the FEA (ANSYS) modal analysis results for a 1D scanner [18]. Mirror vibration frequency requirements determine the flexure beam dimensions that suspend the mirror. Thus, predicting the frequencies for the torsion and other fundamental vibration modes is critical. If torsion is the desired mode, which is the case for microscanners, other modes are often undesired and should be well separated from the torsional mode frequency and its harmonics.

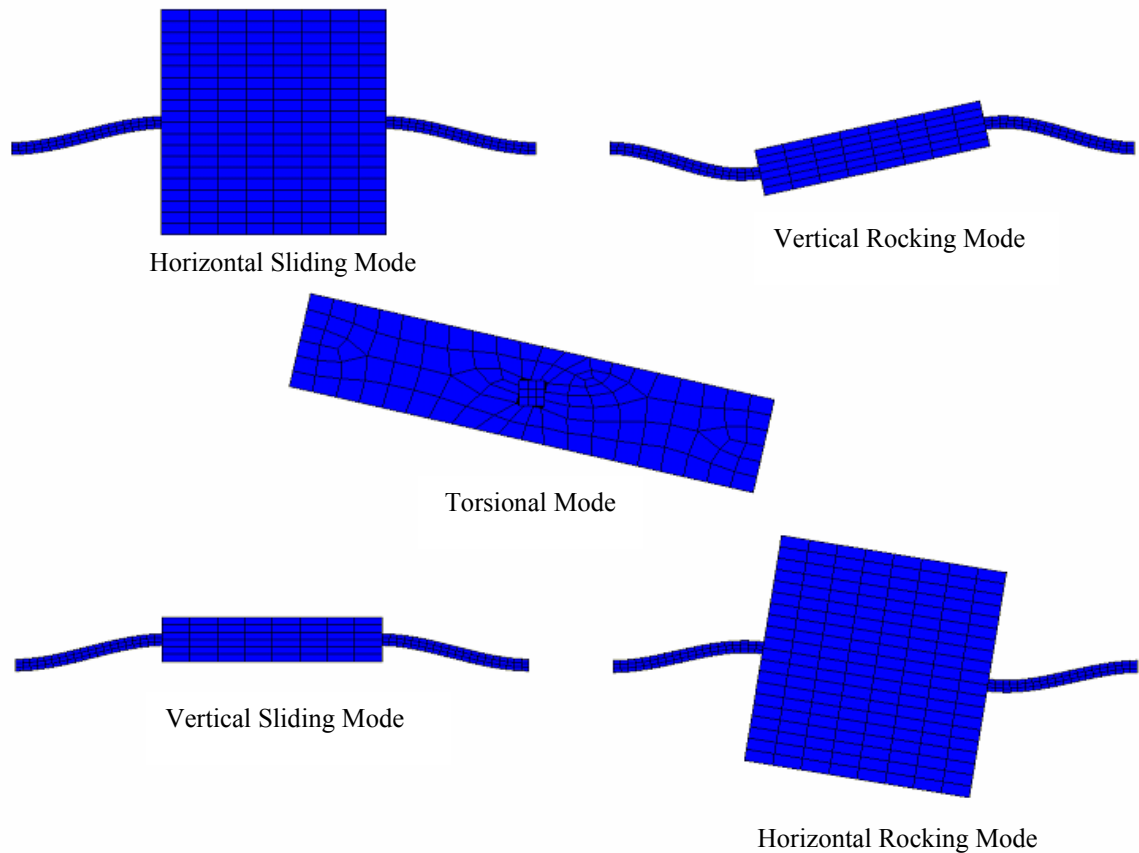


Figure 2.2-2: Five fundamental vibration modes of a box shaped microscanner.

The model consists of 1312 elements and 21294 degrees of freedom. The Lyapunov equation calculations for the disturbance analysis take excessive time for large order systems. In order to reduce the time for the disturbance analysis, this model needs to be simplified without sacrificing its predicting capability of the system behavior. The second FEM is created using beam and shell elements, consisting of 288 elements and 6930 degrees of freedom (see Figure 2.2-3). First 5 natural frequencies are as follows: torsional 5578 Hz, horizontal sliding 9406 Hz, horizontal rocking 10664 Hz, vertical sliding 22726 Hz, vertical rocking 27342 Hz.

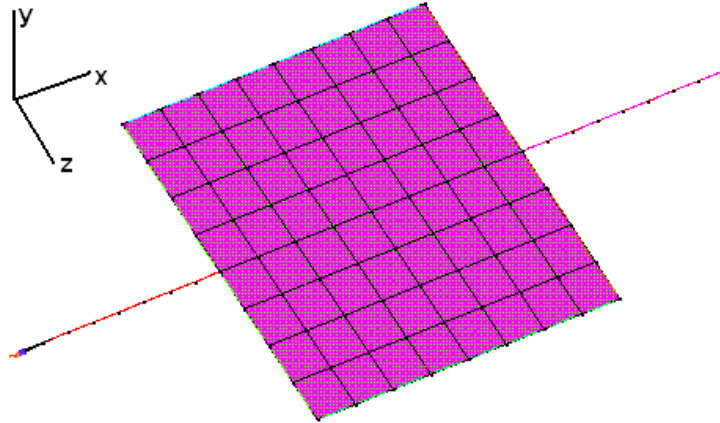


Figure 2.2-3. Simplified finite element model of the MEMS torsional scanner. Beam and shell elements are used for model simplification.

2.3 State-Space Modeling

State-Space representation is a simplified form of the linear differential equation sets [19]. The very well known equation of motion is

$$\mathbf{m}\ddot{\mathbf{x}} + \mathbf{c}\dot{\mathbf{x}} + \mathbf{k}\mathbf{x} = \mathbf{F} \quad (2.12)$$

where \mathbf{m} is mass, \mathbf{c} is damping coefficient, \mathbf{k} is stiffness, and \mathbf{F} is the external force, a second order differential equation. In order to propose a more effective and faster solution technique, the differential equation order is reduced to first order but the number of equations is doubled. Introducing the new variables \mathbf{x}

$$\begin{aligned} \mathbf{x}_1 &= \mathbf{x} \\ \mathbf{x}_2 &= \dot{\mathbf{x}} \end{aligned} \quad (2.13)$$

The differential equation of motion can be written in the form

$$\begin{aligned} \dot{\mathbf{x}}_1 &= \mathbf{x}_2 \\ \dot{\mathbf{x}}_2 &= -\frac{\mathbf{c}}{\mathbf{m}}\mathbf{x}_2 - \frac{\mathbf{k}}{\mathbf{m}}\mathbf{x}_1 + \frac{\mathbf{F}}{\mathbf{m}} \end{aligned} \quad (2.14)$$

Now a second order differential equation is written in the form of two first order differential equations, which is easier to solve. For systems having n degrees of freedom, ' n ' 2nd order differential equations will represent the system. And the state-space representation of this

system will be in the form of '2n' differential equations of first order. Rewriting the system in matrix form

$$\begin{aligned} \begin{bmatrix} \dot{x}_1 \\ \dot{x}_2 \end{bmatrix} &= \begin{bmatrix} \mathbf{0} & \mathbf{1} \\ -\frac{\mathbf{k}}{\mathbf{m}} & -\frac{\mathbf{c}}{\mathbf{m}} \end{bmatrix} \begin{bmatrix} x_1 \\ x_2 \end{bmatrix} + \begin{bmatrix} \mathbf{0} \\ \frac{\mathbf{F}}{\mathbf{m}} \end{bmatrix} \\ y &= [\mathbf{C}] \begin{bmatrix} x_1 \\ x_2 \end{bmatrix} + [\mathbf{D}] \\ \mathbf{A} &= \begin{bmatrix} \mathbf{0} & \mathbf{1} \\ -\frac{\mathbf{k}}{\mathbf{m}} & -\frac{\mathbf{c}}{\mathbf{m}} \end{bmatrix}, \quad \mathbf{B} = \begin{bmatrix} \mathbf{0} \\ \frac{\mathbf{F}}{\mathbf{m}} \end{bmatrix} \end{aligned} \quad (2.15)$$

Also the system output parameter can be defined as the combination of two states defined by the **C** matrix. **D** is the direct transformation matrix which directly effects the output regardless of the states.

ANSYS modal analysis results, eigenvalues and eigenvectors, are used to construct the state-space equations of the mirror. The state-space equations representing the system are,

$$\begin{aligned} \dot{\mathbf{x}}(t) &= \mathbf{A}\mathbf{x}(t) + \mathbf{B}u(t) \\ \mathbf{y}(t) &= \mathbf{C}\mathbf{x}(t) + \mathbf{D}u(t) \end{aligned} \quad (2.16)$$

where

$$\mathbf{A} = \begin{bmatrix} \mathbf{0} & \mathbf{1} & \mathbf{0} & \mathbf{0} & \dots & \dots \\ -\frac{k_1}{m_1} & -\frac{c_1}{m_1} & \mathbf{0} & \mathbf{0} & \dots & \dots \\ \mathbf{0} & \mathbf{0} & \mathbf{0} & \mathbf{1} & \dots & \dots \\ \mathbf{0} & \mathbf{0} & -\frac{k_2}{m_2} & -\frac{c_2}{m_2} & \dots & \dots \\ \dots & \dots & \dots & \dots & \dots & \dots \\ \dots & \dots & \dots & \dots & \dots & \dots \end{bmatrix}$$

$$\mathbf{B} = \begin{bmatrix} 0 \\ 1 \\ 0 \\ 1 \\ \vdots \\ \vdots \end{bmatrix}, \quad \mathbf{C} = [1 \quad 0 \quad 1 \quad 0 \quad \dots \quad \dots] \quad \text{and} \quad \mathbf{D} = [0]. \quad (2.17)$$

In Eqns. 2.17 k_1 and k_2 are first and second natural modes' stiffnesses, and m_1 and m_2 are the modal masses for the corresponding mode shapes as defined in equations 2.10 and 2.11. For example the first mode shape is a torsional mode and the effective stiffness for this mode is the torsional stiffness of flexure beams, while the effective mass is, mainly due to the rotational moment of inertia of the scanner mirror. These are the physical system parameters which are available at the physical coordinate system. The effective stiffness and effective mass are also physical parameters dependent on the design variables which are used to construct the model in the FEM. A new coordinate system called 'the principal coordinate system' may be defined using the system eigenvectors, which are modal analysis results. The 'physical parameters' need to be changed with the 'principal modal parameters' the conversion of physical parameters into principal (modal) parameters is given in Eq 2.9. Using these principal modal parameters state-space matrices can be formed as follows

$$\mathbf{A} = \begin{bmatrix} 0 & 1 & 0 & 0 & \dots & \dots \\ -\omega_1^2 & -2\zeta_1\omega_1 & 0 & 0 & \dots & \dots \\ 0 & 0 & 0 & 1 & \dots & \dots \\ 0 & 0 & -\omega_2^2 & -2\zeta_2\omega_2 & \dots & \dots \\ \dots & \dots & \dots & \dots & \dots & \dots \\ \dots & \dots & \dots & \dots & \dots & \dots \end{bmatrix}$$

$$\mathbf{B} = \Phi^T \begin{bmatrix} 0 \\ 1 \\ 0 \\ 1 \\ \vdots \\ \vdots \end{bmatrix}, \quad \mathbf{C} = \Phi [1 \quad 0 \quad 1 \quad 0 \quad \dots \quad \dots] \quad \text{and} \quad \mathbf{D} = [0]. \quad (2.18)$$

where ω_i is the natural frequency, ζ_i is the damping factor, and Φ is the modal transformation matrix obtained from the ANSYS modal analysis results.

During the dynamic analysis of the microscanner, it was realized that the dynamic behavior is significantly affected by the amount of damping. Thus, it is a critical issue to accurately determine the amount of the damping in MEMS. Damping is the dominant factor that limits the oscillation amplitude of a microscanner. The air between the moving scanner mirror and the stationary part creates an opposing force to the moving device. This resistive force is directly proportional with the mirror angular velocity, and limits the maximum mirror displacement. For such resonating microscanners a damping value of 0.002 of the critical damping may be used. However, experimental methods are available to obtain more accurate values for damping [20].

The state space form in Laplace domain allows the calculation of the transfer functions $\mathbf{H}(s)$, that relates the output rotation, $\mathbf{y}(s)$, to the given torque disturbance inputs, $\mathbf{u}(s)$, such that

$$\mathbf{H}(s) = \frac{\mathbf{y}(s)}{\mathbf{u}(s)} \quad (2.19)$$

We can reduce the size of the matrices by taking only the degree-of-freedom (dofs) associated with the rotation about the flexure axis (x-axis). We are especially interested in the amount of jitter about the x-axis because it is a torsional mirror and it is designed to work in the torsional mode. The results of the ANSYS modal analysis are written to text files and standard MATLAB routines are used to read these files and extract the eigenvectors and eigenvalues to construct the state space matrices.

2.4 Model Reduction

The Lyapunov equation calculations in disturbance analysis (see section 3.1) may take a long time if the full scale FEM is used. We need to reduce the size of the model while still maintaining the desired input/output relations. The MATLAB Control Toolbox has a function “modred” which can be used for reducing models while retaining the overall system dc gain. The “mdc” or “Matched DC” gain option for the function “modred” reduces the selected states

by setting their derivatives to zero, then solving for the remaining states. It is analogous to Guyan reduction because the low frequency effects of the eliminated states are included in the remaining states. The other option for “modred” is the “del” option which simply eliminates the defined states, typically associated with the higher frequency modes. The derivation of the “mdc” option is given in [19] and can be found below.

From the original system \mathbf{x}_r are the states those wanted to be reduced into, and \mathbf{x}_e are the states those are going to be eliminated.

$$\begin{bmatrix} \dot{\mathbf{x}}_r \\ \dot{\mathbf{x}}_e \end{bmatrix} = \begin{bmatrix} \mathbf{A}_{rr} & \mathbf{A}_{re} \\ \mathbf{A}_{re} & \mathbf{A}_{ee} \end{bmatrix} \begin{bmatrix} \mathbf{x}_r \\ \mathbf{x}_e \end{bmatrix} + \begin{bmatrix} \mathbf{B}_r \\ \mathbf{B}_e \end{bmatrix} u \quad (2.20)$$

$$y = \begin{bmatrix} \mathbf{C}_r & \mathbf{C}_e \end{bmatrix} \begin{bmatrix} \mathbf{x}_r \\ \mathbf{x}_e \end{bmatrix} + \mathbf{D}u$$

writing in open form

$$\begin{aligned} \dot{\mathbf{x}}_r &= \mathbf{A}_{rr} \cdot \mathbf{x}_r + \mathbf{A}_{re} \cdot \mathbf{x}_e + \mathbf{B}_r \cdot u \\ \dot{\mathbf{x}}_e &= \mathbf{A}_{er} \cdot \mathbf{x}_r + \mathbf{A}_{ee} \cdot \mathbf{x}_e + \mathbf{B}_e \cdot u \end{aligned} \quad (2.21)$$

truncating the unwanted modes means $\dot{\mathbf{x}}_e = 0$, then

$$0 = \mathbf{A}_{er} \cdot \mathbf{x}_r + \mathbf{A}_{ee} \cdot \mathbf{x}_e + \mathbf{B}_e \cdot u \quad (2.22)$$

taking \mathbf{x}_e to the left hand side

$$\mathbf{x}_e = -\mathbf{A}_{ee}^{-1} \cdot \mathbf{A}_{er} \cdot \mathbf{x}_r - \mathbf{A}_{ee}^{-1} \cdot \mathbf{B}_e \cdot u \quad (2.23)$$

substituting this back into the $\dot{\mathbf{x}}_r$ equation

$$\begin{aligned} \dot{\mathbf{x}}_r &= \mathbf{A}_{rr} \cdot \mathbf{x}_r + \mathbf{A}_{re} \cdot (-\mathbf{A}_{ee}^{-1} \cdot \mathbf{A}_{er} \cdot \mathbf{x}_r - \mathbf{A}_{ee}^{-1} \cdot \mathbf{B}_e \cdot u) + \mathbf{B}_r \cdot u \\ &= (\mathbf{A}_{rr} - \mathbf{A}_{re} \cdot \mathbf{A}_{ee}^{-1} \cdot \mathbf{A}_{er}) \cdot \mathbf{x}_r + (\mathbf{B}_r - \mathbf{A}_{re} \cdot \mathbf{A}_{ee}^{-1} \cdot \mathbf{B}_e) \cdot u \end{aligned} \quad (2.24)$$

so the output equation turns into

$$\begin{aligned} y &= \mathbf{C}_r \cdot \mathbf{x}_r + \mathbf{C}_e \cdot (-\mathbf{A}_{ee}^{-1} \cdot \mathbf{A}_{er} \cdot \mathbf{x}_r - \mathbf{A}_{ee}^{-1} \cdot \mathbf{B}_e \cdot u) + \mathbf{D} \cdot u \\ &= (\mathbf{C}_r - \mathbf{C}_e \cdot \mathbf{A}_{ee}^{-1} \cdot \mathbf{A}_{er}) \cdot \mathbf{x}_r + (\mathbf{D} - \mathbf{C}_e \cdot \mathbf{A}_{ee}^{-1} \cdot \mathbf{B}_e) \cdot u \end{aligned} \quad (2.25)$$

reduce system state space matrices are defined as

$$\begin{aligned}
 \mathbf{A}_{\text{red}} &= \mathbf{A}_{\text{rr}} - \mathbf{A}_{\text{re}} \cdot \mathbf{A}_{\text{ee}}^{-1} \cdot \mathbf{A}_{\text{er}} \\
 \mathbf{B}_{\text{red}} &= \mathbf{B}_{\text{r}} - \mathbf{A}_{\text{re}} \cdot \mathbf{A}_{\text{ee}}^{-1} \cdot \mathbf{B}_{\text{e}} \\
 \mathbf{C}_{\text{red}} &= \mathbf{C}_{\text{r}} - \mathbf{C}_{\text{e}} \cdot \mathbf{A}_{\text{ee}}^{-1} \cdot \mathbf{A}_{\text{er}} \\
 \mathbf{D}_{\text{red}} &= \mathbf{D} - \mathbf{C}_{\text{e}} \cdot \mathbf{A}_{\text{ee}}^{-1} \cdot \mathbf{B}
 \end{aligned}
 \tag{2.26}$$

In the original space state equations \mathbf{D} , direct transmission matrix, is equal to zero, however when reducing the model (not truncating) there comes an extra $\mathbf{D} - \mathbf{C}_{\text{e}} \cdot \mathbf{A}_{\text{ee}}^{-1} \cdot \mathbf{B}$ term. This yields a different characteristic for the frequency response, which does not capture the behavior at higher frequencies.

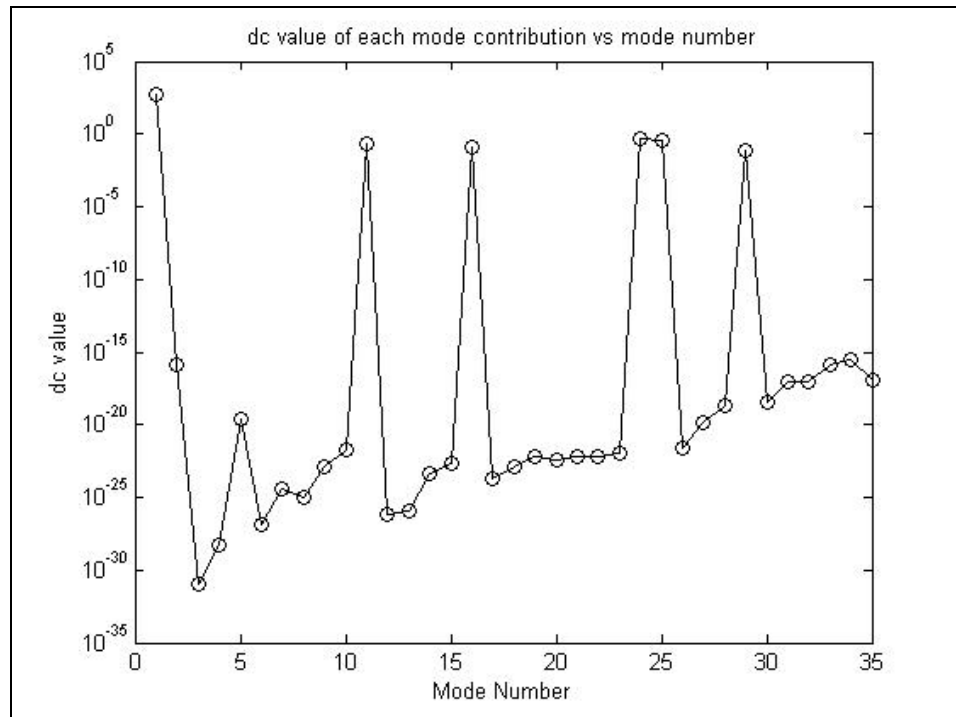


Figure 2.4-1. dc gain values plotted for each mode, the first mode being the torsional mode has the greatest dc gain among all

An alternative method is called the “dc gain” and “peak gain” approach. ‘dc’ gain (for damped and undamped cases) is defined as

$$dcgain = \frac{y_{ji}}{u_{ki}} = \frac{y_{nji} \cdot y_{nki}}{\omega_i^2}
 \tag{2.27}$$

where $y_{nji} \cdot y_{nki}$ is the product of the j^{th} (output) row and k^{th} (force applied) row terms of the i^{th} eigenvector divided by the square of the eigenvalue for the i^{th} mode.

At resonances, the peak gain amplitude of each mode is given by the formula:

$$\begin{aligned} peakgain &= \frac{y_{ji}}{u_{ki}} = \frac{-j}{2\zeta} \frac{y_{nji} \cdot y_{nki}}{\omega_i^2} \\ &= \frac{-j}{2\zeta} (dcgain) \end{aligned} \quad (2.28)$$

If the same value of ζ is used for all modes, then all the dc gain terms are divided by the same 2ζ terms and the relative amplitudes of the dc gains and peak gains are the same, so there is no difference between sorting a uniform damping model using “dc gain” or “peak gain”.

The results of the two reduction methods are shown in Figures 2.4-2 and 2.4-3. Figure 2.4-2 shows the frequency response of the overall system for “del” “modred” option, where all the modes above 27342 Hz are eliminated (only 6 lowest modes are kept). As it is expected, it does not capture the higher frequency modes since they are not included in the calculations. Figure 2.4-3 shows the results of sorting the modes according to the “dc gain” and “peak gain” approach. Although the size of the state space model has been decreased significantly (e.g. Size of the matrix A is reduced from 210x210 to 12x12), the reduced model captures all the significant dynamics. This method is found to be the most efficient way to reduce the state space model of the mirror for the transfer function of interest and reduced model obtained with this technique will be used for the remaining part of this study.

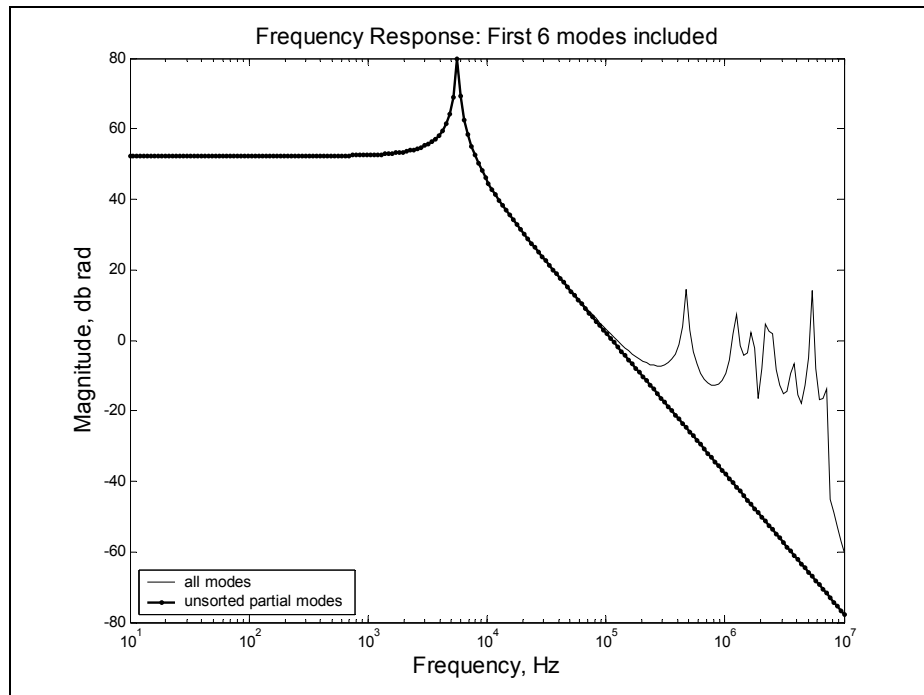


Figure 2.4-2: First six modes are used to construct the reduced model.

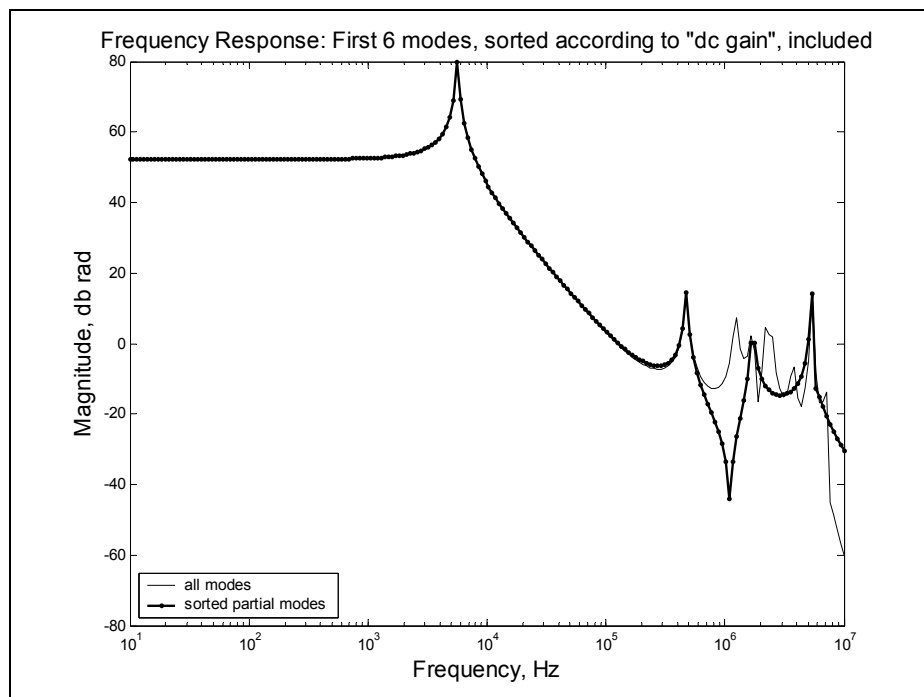


Figure 2.4-3: Modes are sorted according to the "dc gain" and "peak gain" approach.

First six modes with higher gains are used to construct the reduced model.

Chapter 3

DISTURBANCE ANALYSIS FRAMEWORK

3.1 Introduction

After developing a reduced, state-space model of the physical system using FEA results, as described in the previous chapter, the next step is to predict the performance when the model is subjected to the anticipated disturbances. The performance of optical microsystems is directly related to its ability to steer the light beam in the desired direction. In this study, the performance is defined as the rotation of the mirror about the x-axis. The variance of this rotation angle under the effect of a disturbance torque is important. This variance should be kept as small as possible in order to improve the performance of the mirror. Disturbance analyses are usually conducted in order to predict the effect of disturbances on system outputs of interest. The disturbances can be modeled in a number of forms, and as a result, various types of disturbance analyses can be performed.

In this study, two different approaches for disturbance analysis are discussed. These are Lyapunov analysis and time domain analysis. The Lyapunov approach uses the state space model where a lumped single degree of freedom model is used in the time domain analysis.

3.2 Disturbance Analysis using Lyapunov Approach

For stochastic linear systems driven by white noise, the solution of the Lyapunov equation represents the variance of the state vector [21]. The disturbance torque is modeled as the output of a first order shaping filter which is driven by unit intensity white noise.

When assessing the impact of disturbances on high-performance systems, it is critical that the disturbance models should be representative of the actual disturbances. An accurate plant model can still produce incorrect results when improperly modeled disturbances are applied to it. If design trades and decisions are based on the results of disturbance analyses that use mismodeled disturbances, the performance of the actual system in operation might be quite different from that which was predicted. As a result, the disturbance characterization process should be given as high a priority as the modeling process. This is especially true for high performance systems such as MEMS devices in which even low disturbance levels can cause the response to exceed requirements.[16]

Disturbances can be quantified by their frequency content, magnitude level, and the location and direction at which they enter the structure. The frequency content determines which modes of the structure can be excited and what the bandwidth of a control system should be. The magnitude level determines how much energy enters the structure. The location and direction information determine to what extent the modes in the frequency range can be excited.

In this study, we will induce the disturbances as the outputs of a shaping filter. The disturbance filter can be modeled in state-space form as (see Figure 3.2-1).

$$\begin{aligned}\dot{\mathbf{x}}_d(t) &= \mathbf{A}_d \mathbf{x}_d(t) + \mathbf{B}_d \cdot \mathbf{x}_d(t) \\ u(t) &= \mathbf{C}_d \cdot \mathbf{x}_d(t)\end{aligned}\quad (3.3)$$

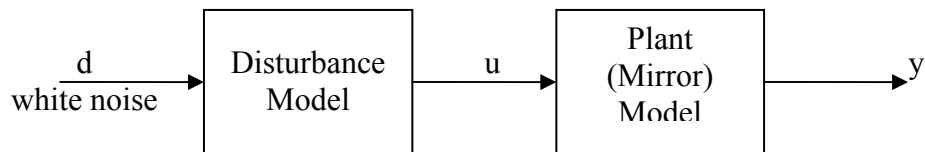


Figure 3.2-1: Disturbance shaping filter connected in series with the mirror model.

The frequency content of the disturbances is constituted by defining a corner frequency for the disturbance filter. The frequency response of the constructed disturbance system is shown in the Figure 3.2-2. Ogata [22] showed that the logarithmic representation of the frequency-response curve can be approximated by two straight-line asymptotes, one a straight line at '0' dB and the other a straight line with a slope '-20dB/decade' (or '-6dB/octave'). The frequency at which two asymptotes meet is called the corner frequency (or break frequency). The corner frequency is indicated on the Figure 3.2-2, which is '251 rad/sec' about '40 Hz'. The effect of the corner frequency can be better understood if Figure 3.2-3 is observed carefully. Different corner frequencies are applied to the same filter, one at 10Hz and other at 10kHz. The filter is fed with a white noise signal. The blue line corresponds to 10 Hz corner frequency which means that faster than 10 Hz the magnitude of the input signal will be attenuated by the filter. Conversely the red line corresponds to 10 kHz corner frequency, the magnitude stays still up to 10 kHz. The corner frequency of the created disturbance filter is 40Hz,

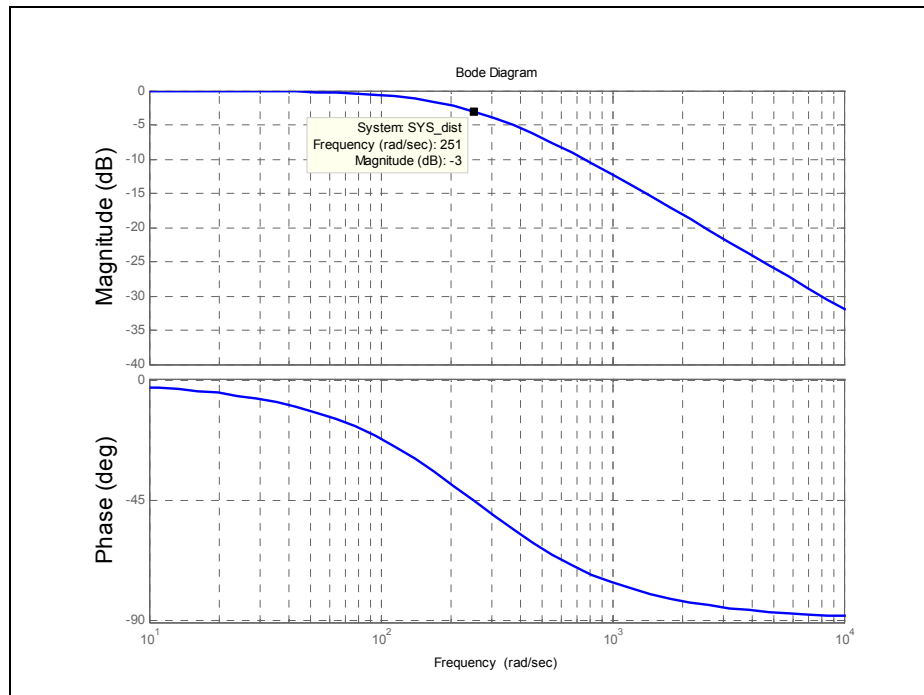


Figure 3.2-2: The frequency response and phase diagrams for the disturbance filter. The magnitude falls down quickly after the corner frequency (2510rad/sec \sim 400Hz).

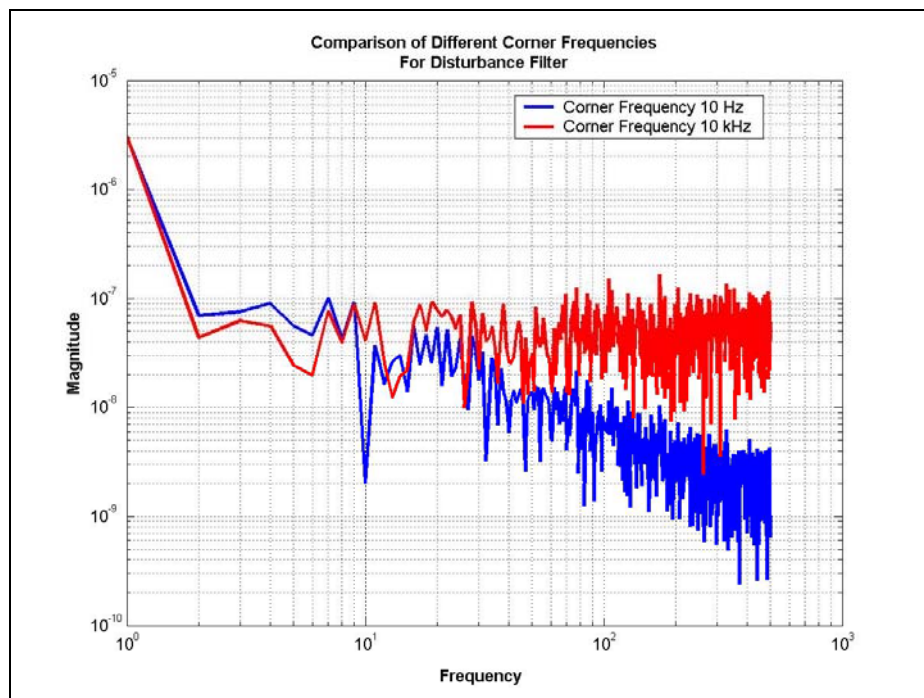


Figure 3.2-3: Comparison of Different Corner Frequencies For Disturbance Filter

The magnitude level of the disturbances are obtained experimentally. Chapter 5 summarizes the experimental procedure and its application in disturbance analysis framework. The magnitude content of the disturbance shaping filter is defined with a constant ‘Disturbance Torque Intensity’. Torque intensity is used to scale the unit intensity white noise into the desired magnitude of the disturbance torques.

Placing the state-space form of the disturbance filter in series with the plant equations from Eq.3.2, an overall system of the form

$$\begin{aligned}\dot{\mathbf{x}}(t) &= \mathbf{A}_{zd}\mathbf{x}(t) + \mathbf{B}_{zd}d(t) \\ \mathbf{y}(t) &= \mathbf{C}_{zd}\mathbf{x}(t)\end{aligned}\quad (3.2)$$

can be represented.

Solution of the following steady-state Lyapunov equation leads to the state covariance matrix Σ_q .

$$\mathbf{A}_{zd}\Sigma_q + \Sigma_q\mathbf{A}_{zd}^T + \mathbf{B}_{zd}\mathbf{B}_{zd}^T = 0 \quad (3.3)$$

This is a matrix equation with the unknown matrix Σ_q , and solution techniques are available through standard commercial software packages such as MATLAB. It should be emphasized that Σ_q represents the *steady-state* covariance matrix. One can imagine that if the stochastic disturbances d (see Figure 3.2-1) are suddenly applied to the system, there will be a period when transient behavior is dominant and the performance outputs are not steady state, so the above solution does not apply but a dynamical version of the Lyapunov equation represents the system for this case

$$\mathbf{A}_{zd}\Sigma_q(t) + \Sigma_q(t)\mathbf{A}_{zd}^T + \mathbf{B}_{zd}\mathbf{B}_{zd}^T = \dot{\Sigma}_q(t) \quad (3.4)$$

and it is assumed that the initial state covariance matrix Σ_{q0} is specified. When these transient effects decay away, the outputs can be characterized as stationary random processes with a covariance matrix equal to Σ_q .

The performance covariance matrix is given by

$$\Sigma_z = \mathbf{C}_{zd} \Sigma_q \mathbf{C}_{zd}^T \quad (3.5)$$

and the root-mean-square (RMS) values of the performance metrics can be obtained from the square roots of the diagonal entries of the matrix

$$\Sigma_z = \begin{bmatrix} \sigma_{z1}^2 & \sigma_{z1z2} & \cdots & \sigma_{z1zn} \\ \sigma_{z2z1} & \sigma_{z2}^2 & \cdots & \sigma_{z2zn} \\ \vdots & \vdots & \ddots & \vdots \\ \sigma_{znz1} & \sigma_{znz2} & \cdots & \sigma_{zn}^2 \end{bmatrix} \quad (3.6)$$

Using the Lyapunov approach RMS estimates (in the sense of statistical steady state) can be calculated easily and directly by solving a single matrix equation. It provides the exact mean-square values of the performance variables with subject to the accuracy of the disturbance and plant models. The diagonal terms of Σ_z represent the mean-square values σ_{zi}^2 , and the root-mean-square (RMS) values are simply σ_{zi} [16].

There are some shortcomings of the presented Lyapunov approach; first of all it does not provide any direct insight into the frequency content of the outputs. Rather, it yields the overall variances of the states and the outputs. In addition to that, the solution time for the Lyapunov equation can be excessive for large-order systems. In such cases, model reduction should first be performed to bring the number of states to a reasonable level without sacrificing the predictive capability of the model. Some model reduction techniques, discussed in the previous chapter, are available for an acceptable reduction of the model.

The disturbance analysis of the mirror is conducted with an external disturbance torque acting on the mirror. As we had mentioned at the beginning, quantifying the disturbances for MEMS devices is important in order to predict their performances accurately. But at the same time, measuring and modeling these disturbances is a very tedious process since they can vary depending on the electronics or sensors used.

3.3 Disturbance Analysis in Time Domain

Same system properties are used to construct a lumped mass-spring-damper system (see Figure 3.3-1). The stiffness and inertia terms are calculated using formulation derived by Urey [23]. The purpose of creating such a model is solving the same disturbance problem in the time domain and comparing the results of the two methods.

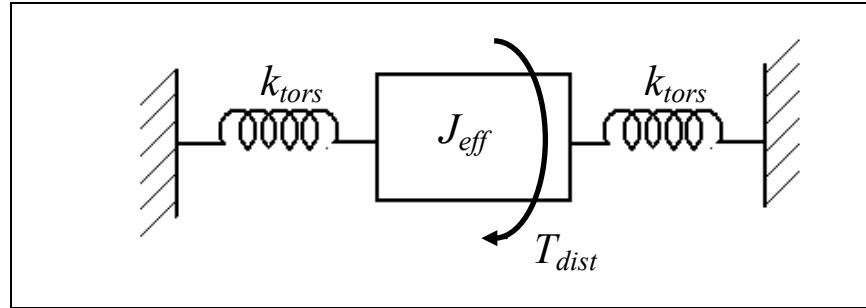


Figure 3.3-1: Lumped mass-spring-damper model

The lumped system can be represented with the following equation:

$$\ddot{\theta} + \frac{b}{J_{eff}} \dot{\theta} + \frac{k_{tors}}{J_{eff}} \theta = \frac{T_{dist}}{J_{eff}} \quad (3.7)$$

where θ is the tilt angle of the lumped mirror model, b is the damping of the system, k_{tors} is the torsional stiffness of the flexure beams, J_{eff} is the effective inertia of the scanner, and T_{dist} is the disturbance torque applied due to the environmental disturbances. See Table 3.3-1 and Table 3.3-2 for k_{tors} and J_{eff} formulas.

Table 3.3-1: Effective mass moment of inertia and effective stiffness terms for the torsional mode of a torsional scanner

Effective Moment of Inertia*	Effective Stiffness **
$J_{eff} = J_{m,xx} + \frac{2}{3} J_{f,xx}$ $J_{f,xx} = \frac{1}{3} M_f (a^2 + b^2)$	$k_{tors} = \frac{2GK}{L_f}, \quad \mu = \sqrt{G_{xz} / G_{xy}}$ $GK = \begin{cases} (ab^3 Gxy) \left[5.33 - 3.36 \frac{b}{a\mu} \left(1 - \frac{b^4}{12a^4 \mu^4} \right) \right] & a\mu \geq b \\ (ab^3 Gxy) \left[5.33 - 3.36 \frac{a\mu}{b} \left(1 - \frac{b^4}{12a^4 \mu^4} \right) \right] & a\mu < b \end{cases}$

*: For mass moment of inertia terms check Table 3.3-2

Table 3.3-2: Mass and mass moment of inertia terms for a rectangular mirror geometry

Mirror Mass	Mass Moment of Inertia
$M_m = \rho L_m D t_m$	$J_{m,xx} = \frac{M_m}{12} (D^2 + t_m^2)$

' a ', ' b ' and ' L_f ' are half width, height and length of the flexure beams, respectively. G_{xy} and G_{xz} are shear modulus of elasticity. The lumped model is excited with random forces which can be assumed to be the disturbances [24]. An array of random numbers are created and normalized to unity then they are multiplied with the measured disturbance torque magnitude. Disturbance time history is given in Figure 3.3-2. Numerical integration of Eq. 3.7 can be performed using MATLAB built-in function "lsim". Integrating randomly excited system on time provides the time versus angular displacement plot which then can be used to calculate the RMS value of the angular displacement of the disturbed system. Angular displacement of the mirror is given as a function of time in Figure 3.3-3.

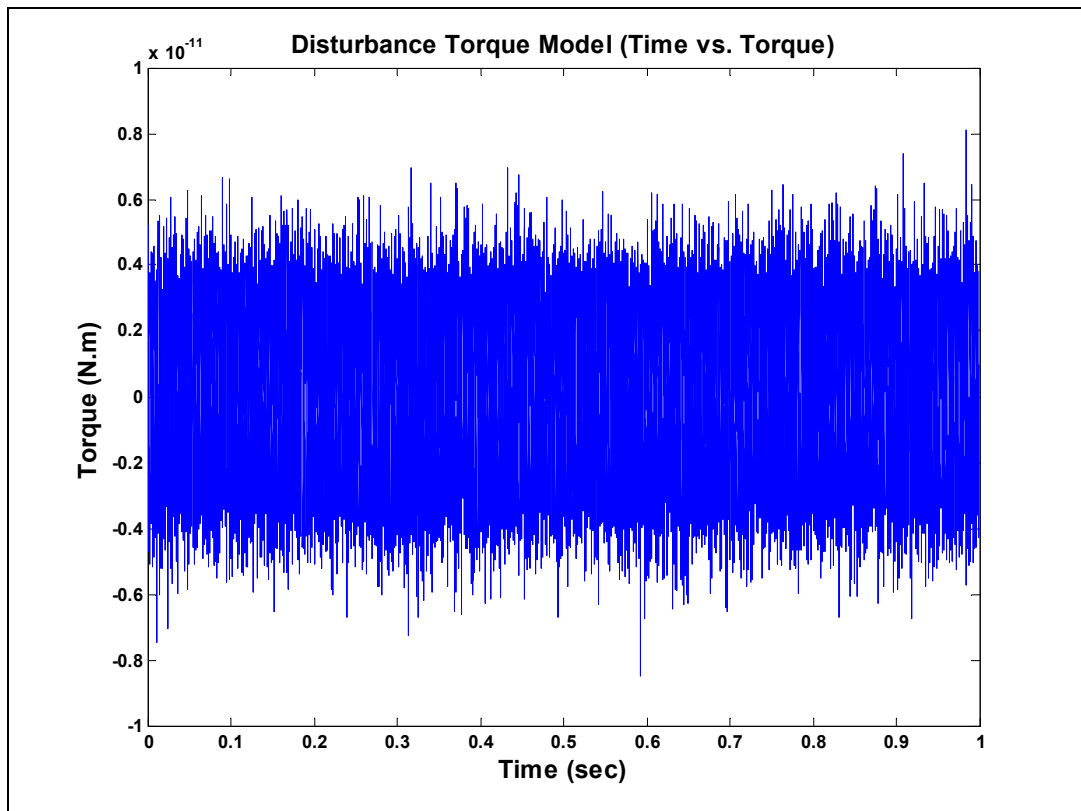


Figure 3.3-2: Time history of the disturbances. A randomly generated number array then scaled down to the expected disturbances' magnitude level.

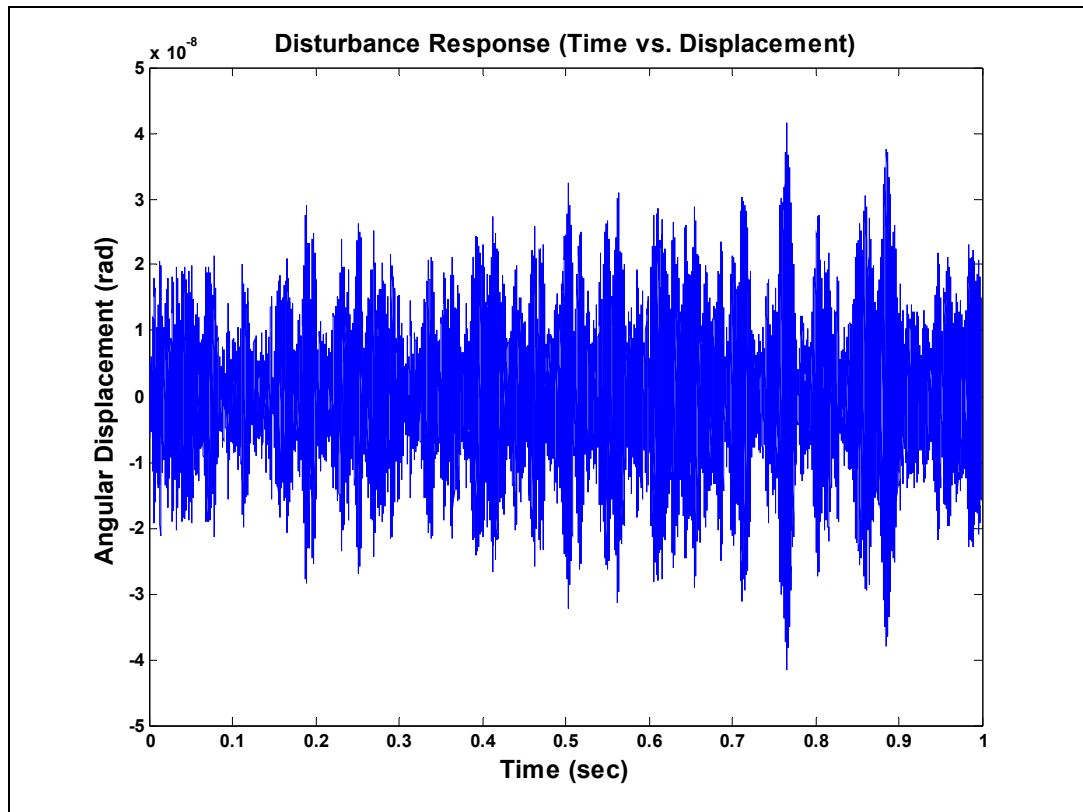


Figure 3.3-3: The angular displacement as a function of time. The equation of motion representing the lumped system is integrated using the MATLAB function 'lsim'. The torque input is a randomly created disturbance array

The results of the Lyapunov approach and the time domain analysis are compared and they are found to be on the same order of magnitude (See Table 3.3-3). The time domain analysis proved that the Lyapunov approach is a very accurate and very efficient method to calculate the jitter of the mirror when it is exposed to random disturbances.

Table 3.3-3 Comparison of Lyapunov approach and time domain analysis.

RMS value of the mirror angular displacement	Lyapunov Approach (rad)	Lumped Model (rad)
	1.75×10^{-8}	1.27×10^{-8}

The tilting angle of the micro mirror is defined as the mechanical scan angle. The mechanical scan angle is given as 5° in [30]. If this system is used to write a SVGA (800x600) display then 600 lines will be written with this 5° scan angle. Therefore the amount of radians corresponding to a line can be calculated using the following equation, and it is found to be 1.45×10^{-4} .

$$\frac{5^\circ \cdot 2\pi}{360^\circ} = 0.087 \text{ rad}, \quad \frac{0.087 \text{ rad}}{600} = 1.45 \times 10^{-4} \text{ rad} \quad (3.8)$$

The display is not acceptable if the pixels are distorted by an amount of 20% [27].

$$1.45 \times 10^{-4} \text{ rad} \cdot 20/100 = 2.9 \times 10^{-5} \text{ rad} \quad (3.9)$$

As a result an absolute value of the variation of the mirror rotation should be smaller than the value found in equation 3.9. Only then, the written display quality is acceptable. The disturbance analysis results are significantly smaller than the required display quality value. The environmental and driving electronics' disturbances are not impacting the quality of the display image, according to our newly developed disturbance analysis tool.

Chapter 4

SENSITIVITY ANALYSIS FRAMEWORK

4.1 Introduction

Although there are newly developed design tools in MEMS area, there is always a probability of a design not to meet the specified requirements. Predicting and improving the performance of a certain design before production provides countless benefits. Sensitivity analysis is one of the design techniques that can be used to identify the critical design parameters for optimizing the performance of a system. Sensitivity information provides the performance change of a system with respect to the changing design parameters.

This chapter combines the disturbance analysis framework with the sensitivity analysis framework. The sensitivity analysis is demonstrated through a case study which includes the sensitivity analysis of a torsional MEMS scanner mirror (see Figure 4.1-1).

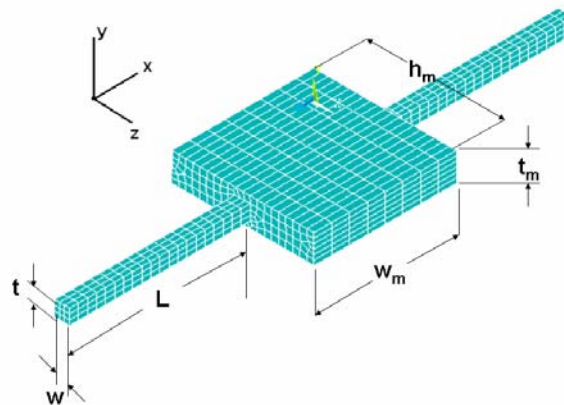


Figure 4.1-1: Torsional MEMS Scanner showing the design parameters

Sensitivity analysis is an intermediate tool between design and redesign stages. Especially, when a system does not satisfy specified performance requirements, sensitivity information can identify which components in the system are important.

4.2 Sensitivity Analysis Framework

Determining sensitivity of design parameters can provide useful information when the system does not meet the specified requirements. For systems with many design parameters, sensitivity information can identify which parameters in the system are the most significant. These parameters might be the focus of redesign efforts that attempt to improve the performance.

This section describes the mathematical theory for computing sensitivities when the system is written in state-space form. The state-space equations of the torsional MEMS scanner can be represented in the matrix form [16]

$$\begin{aligned}\dot{\mathbf{x}}(t) &= \mathbf{A}\mathbf{x}(t) + \mathbf{B}u(t) \\ \mathbf{y}(t) &= \mathbf{C}\mathbf{x}(t) + \mathbf{D}u(t)\end{aligned}\quad (4.1)$$

where $\mathbf{y}(t)$ is the output or equivalently the performance of the mirror about the scanning axis due to the given input disturbance torque. Placing this state-space system in series with the disturbance state-space equations, an overall system of the form can be represented as follows:

$$\begin{aligned}\dot{\mathbf{x}}(t) &= \mathbf{A}_{zd}\mathbf{x}(t) + \mathbf{B}_{zd}d(t) \\ \mathbf{y}(t) &= \mathbf{C}_{zd}\mathbf{x}(t)\end{aligned}\quad (4.2)$$

Solution of the following steady-state Lyapunov equation leads to the state covariance matrix Σ_q .

$$\mathbf{A}_{zd}\Sigma_q + \Sigma_q\mathbf{A}_{zd}^T + \mathbf{B}_{zd}\mathbf{B}_{zd}^T = 0 \quad (4.3)$$

This is a matrix equation with the unknown matrix Σ_q , and it can be solved using MATLAB.

The performance covariance matrix is given by

$$\Sigma_z = \mathbf{C}_{zd}\Sigma_q\mathbf{C}_{zd}^T \quad (4.4)$$

where Σ_z is a square matrix containing the mean square values of the performance metrics σ_{zi}^2 at its diagonal entries; σ_{zi}^2 occurs in Equation 4.5 writing this equation only for an interested performance metric,

$$\sigma_{zi}^2 = \mathbf{C}_{zi}\Sigma_q\mathbf{C}_{zi}^T \quad (4.5)$$

these can be used to calculate the exact root mean square (RMS) values of the performance variables.

In order to compute the sensitivities following expression must be evaluated;

$$\frac{\partial \sigma_{zi}}{\partial p} = \text{Sensitivity of a performance RMS with respect to parameter } p \quad (4.6)$$

The first step is to find the derivative of the variance σ_{zi}^2 with respect to p . Taking the derivative of Eq. 4.4 with respect to p is not possible because Σ_q is the solution to Eq. 4.3; therefore, Σ_q is implicitly dependent on p . To get around this problem, it is possible to use the Lagrange Multiplier method, treat the Lyapunov equation Eq. 4.3 as a constraint equation, and augment it to Eq. 4.4 with the help of a symmetric Lagrange multiplier matrix. The Lagrange multiplier method was applied to modal and physical parameter sensitivity problems by Gutierrez [16] and the resulting equations for sensitivity calculations are presented in the following sections. As suggested by Gutierrez, the problem is going to be separated into two sections. The first one will be to perform the modal parameter sensitivity analysis and the second will be the physical parameter sensitivity analysis.

4.2.1 Lagrange Multiplier Method

The Lagrange Multiplier Method of optimization is named for its developer Joseph Louis Lagrange (1746-1814), a French mathematician and astronomer [25]. This method is important when dealing with nonlinear optimization problems. It uses a function called the ‘Lagrange Expression’ or ‘Lagrangian’, LE, $(\sigma_{zi}^2)^*$ in our problem, which consists of the objective function $U(x,y,z)$, σ_{zi}^2 in our case, and constraint functions, $h_i(x,y,z)$, Lyapunov Equation in our case, multiplied by Lagrange multipliers, L_i .

$$LE = U(x,y,z) + L_1 \cdot h_1(x,y,z) + L_2 \cdot h_2(x,y,z) + \dots + L_i \cdot h_i(x,y,z) \quad (4.7)$$

The additional unknown, L_i is introduced into the Lagrange expression so that in determining the optimum values of x , y , z the problem can be treated as though it was unconstrained. The conditions that must be satisfied for the optimum points are as follows.

$$\begin{aligned} \frac{\partial LE}{\partial x} = 0, \quad \frac{\partial LE}{\partial y} = 0, \quad \frac{\partial LE}{\partial z} = 0, \\ \frac{\partial LE}{\partial L_1} = 0, \quad \frac{\partial LE}{\partial L_2} = 0 \dots \quad \frac{\partial LE}{\partial L_i} = 0 \end{aligned} \quad (4.8)$$

where ‘ i ’ is the number of Lagrange Multipliers.

Returning back to the sensitivity analysis problem, it is stated that treating the Lyapunov equation, Eq.4.3 as a constraint equation, and augmenting it to Eq.4.4 via a symmetric Lagrange

multiplier matrix L_i is a solution. (A subscript i is used since there will be a different matrix for every performance metric.) The notation $(\sigma_{zi}^2)^*$ is used to denote the Lagrangian of σ_{zi}^2 . In addition to that “trace” is the summation of the diagonal terms of the matrix represented by $L_i(\mathbf{A}_{zd} \cdot \boldsymbol{\Sigma}_q + \boldsymbol{\Sigma}_q \cdot \mathbf{A}_{zd}^T + \mathbf{B}_{zd} \cdot \mathbf{B}_{zd}^T)$

$$\begin{aligned} (\sigma_{zi}^2)^* &= \sigma_{zi}^2 \\ &+ \text{trace}\left[L_i(\mathbf{A}_{zd} \cdot \boldsymbol{\Sigma}_q + \boldsymbol{\Sigma}_q \cdot \mathbf{A}_{zd}^T + \mathbf{B}_{zd} \cdot \mathbf{B}_{zd}^T)\right] \\ &= \mathbf{C}_{zi} \cdot \boldsymbol{\Sigma}_q \cdot \mathbf{C}_{zi}^T \\ &+ \text{trace}\left[L_i(\mathbf{A}_{zd} \cdot \boldsymbol{\Sigma}_q + \boldsymbol{\Sigma}_q \cdot \mathbf{A}_{zd}^T + \mathbf{B}_{zd} \cdot \mathbf{B}_{zd}^T)\right] \end{aligned} \quad (4.9)$$

The derivative of the variance σ_{zi}^2 with respect to p is equal to the derivative of the Lagrangian function if and only if the derivatives with respect to $\boldsymbol{\Sigma}_q$ and L_i are equal to zero.

$$\frac{\partial \sigma_{zi}^2}{\partial p} = \frac{\partial (\sigma_{zi}^2)^*}{\partial p} \bigg|_{\substack{\frac{\partial (\sigma_{zi}^2)^*}{\partial L_i} = 0, \\ \frac{\partial (\sigma_{zi}^2)^*}{\partial \boldsymbol{\Sigma}_q} = 0}} \quad (4.10)$$

The derivative with respect to L_i is,

$$\frac{\partial (\sigma_{zi}^2)^*}{\partial L_i} = \frac{\partial}{\partial L_i} \text{trace}\left[L_i(\mathbf{A}_{zd} \cdot \boldsymbol{\Sigma}_q + \boldsymbol{\Sigma}_q \cdot \mathbf{A}_{zd}^T + \mathbf{B}_{zd} \cdot \mathbf{B}_{zd}^T)\right] \quad (4.11)$$

$$\begin{aligned} \frac{\partial (\sigma_{zi}^2)^*}{\partial L_i} &= \frac{\partial}{\partial L_i} \text{trace}\left[L_i \cdot \mathbf{A}_{zd} \cdot \boldsymbol{\Sigma}_q\right] \\ &+ \frac{\partial}{\partial L_i} \text{trace}\left[L_i \cdot \boldsymbol{\Sigma}_q \cdot \mathbf{A}_{zd}^T\right] \\ &+ \frac{\partial}{\partial L_i} \text{trace}\left[L_i \mathbf{B}_{zd} \cdot \mathbf{B}_{zd}^T\right] = 0 \end{aligned} \quad (4.12)$$

Following the matrix derivative formula results

$$\frac{\partial (\sigma_{zi}^2)^*}{\partial L_i} = \boldsymbol{\Sigma}_q \cdot \mathbf{A}_{zd}^T + \mathbf{A}_{zd} \cdot \boldsymbol{\Sigma}_q + \mathbf{B}_{zd} \cdot \mathbf{B}_{zd}^T = 0 \quad (4.13)$$

Similarly the derivative with respect to $\boldsymbol{\Sigma}_q$ is,

$$\frac{\partial (\sigma_{zi}^2)^*}{\partial \boldsymbol{\Sigma}_q} = \frac{\partial}{\partial \boldsymbol{\Sigma}_q} \text{trace}\left[\begin{aligned} &\mathbf{C}_{zi} \cdot \boldsymbol{\Sigma}_q \cdot \mathbf{C}_{zi}^T \\ &+ L_i(\mathbf{A}_{zd} \cdot \boldsymbol{\Sigma}_q + \boldsymbol{\Sigma}_q \cdot \mathbf{A}_{zd}^T + \mathbf{B}_{zd} \cdot \mathbf{B}_{zd}^T) \end{aligned}\right] \quad (4.14)$$

$$\begin{aligned} \frac{\partial(\sigma_{zi}^2)^*}{\partial \Sigma_q} &= \frac{\partial}{\partial \Sigma_q} \text{trace}[\mathbf{C}_{zi} \cdot \Sigma_q \cdot \mathbf{C}_{zi}^T] \\ &+ \frac{\partial}{\partial \Sigma_q} \text{trace}[L_i \cdot \mathbf{A}_{zd} \cdot \Sigma_q] + \frac{\partial}{\partial \Sigma_q} \text{trace}[L_i \cdot \Sigma_q \cdot \mathbf{A}_{zd}^T] = 0 \end{aligned} \quad (4.15)$$

Following the matrix derivative formula for the above equation and making the use of the fact that L_i is symmetric leads to

$$\frac{\partial(\sigma_{zi}^2)^*}{\partial \Sigma_q} = \mathbf{C}_i^T \mathbf{C}_i + L_i \cdot \mathbf{A}_{zd} + \mathbf{A}_{zd}^T \cdot L_i = 0 \quad (4.16)$$

This produces another Lyapunov equation that is used to determine L_i .

$$L_i \cdot \mathbf{A}_{zd} + \mathbf{A}_{zd}^T \cdot L_i + \mathbf{C}_i^T \mathbf{C}_i = 0 \quad (4.17)$$

Finally taking the derivative of (4.9) with respect to p leads to

$$\begin{aligned} \frac{\partial \sigma_{zi}^2}{\partial p} &= \text{trace} \left[\Sigma_q \frac{\partial(\mathbf{C}_{zi} \cdot \mathbf{C}_{zi}^T)}{\partial p} \right] \\ &+ \text{trace} \left[L_i \cdot \left(\frac{\partial \mathbf{A}_{zd}}{\partial p} \cdot \Sigma_q + \Sigma_q \frac{\partial \mathbf{A}_{zd}^T}{\partial p} + \frac{\partial(\mathbf{B}_{zd} \cdot \mathbf{B}_{zd}^T)}{\partial p} \right) \right] \end{aligned} \quad (4.18)$$

Above equations contain derivative terms of \mathbf{A}_{zd} with respect to parameter p . Here p can be a physical parameter as well as a modal parameter. If p is a physical parameter since \mathbf{A}_{zd} and \mathbf{C}_{zd} is constructed using modal analysis results, evaluating the derivative requires the derivatives of the eigenvector and eigenvalues to be calculated. However p being a modal parameter (ω_j , j^{th} natural frequency or ζ , modal damping) makes life easier in the sense of calculating the derivatives of state-space elements \mathbf{A}_{zd} and \mathbf{C}_{zd} . Therefore the sensitivity analysis is first conducted using modal parameters.

4.2.2 Modal Parameter Sensitivities Using Analytical Approach

While the modal sensitivities do identify which modes are the most important, they do not reveal directly what physical characteristics of the design should be modified to affect the modes and improve the design. The sensitivity calculation with respect to a modal parameter is the first step to calculate the physical parameter sensitivities. In this study, the modal parameter is chosen to be the j^{th} natural frequency ω_j . Since the state-space system is constructed in the modal form, it is easy to calculate the system sensitivities with respect to the modal parameters.

\mathbf{A}_{zd} matrix in Eq. 4.2 can be written as follows

$$\mathbf{A}_{zd} = \begin{bmatrix} \mathbf{A} & \mathbf{BC}_d \\ \mathbf{0} & \mathbf{A}_d \end{bmatrix} \quad (4.19)$$

where the plant matrix \mathbf{A} is,

$$\mathbf{A} = \begin{bmatrix} 0 & 1 & 0 & 0 & \dots & \dots \\ -\omega_1^2 & -2\zeta_1\omega_1 & 0 & 0 & \dots & \dots \\ 0 & 0 & 0 & 1 & \dots & \dots \\ 0 & 0 & -\omega_2^2 & -2\zeta_2\omega_2 & \dots & \dots \\ \dots & \dots & \dots & \dots & \dots & \dots \\ \dots & \dots & \dots & \dots & \dots & \dots \end{bmatrix} \quad (4.20)$$

It can be easily differentiated with respect to the modal parameter ω_j (i.e. $j=1$).

$$\frac{\partial \mathbf{A}_{zd}}{\partial \omega_1} = \begin{bmatrix} 0 & 0 & 0 & 0 & \dots & \dots \\ -2\omega_1 & -2\zeta_1 & 0 & 0 & \dots & \dots \\ 0 & 0 & 0 & 0 & \dots & \dots \\ 0 & 0 & 0 & 0 & \dots & \dots \\ \dots & \dots & \dots & \dots & \dots & \dots \\ \dots & \dots & \dots & \dots & \dots & \dots \end{bmatrix} \quad (4.21)$$

The matrix derivatives with respect to ω_j consist entirely of zeros except at the location where those specified modal parameters appear.

The only state-space element including a modal element is the \mathbf{A} matrix, therefore the sensitivity solution reduces to

$$\frac{\partial \sigma_{zi}}{\partial p} = \frac{1}{2\sigma_{zi}} \text{trace} \left[L_i \cdot \left(\frac{\partial \mathbf{A}_{zd}}{\partial p} \boldsymbol{\Sigma}_q + \boldsymbol{\Sigma}_q \frac{\partial \mathbf{A}_{zd}^T}{\partial p} \right) \right] \quad (4.22)$$

where $\boldsymbol{\Sigma}_q$ is the steady state covariance matrix, which is the solution of the Lyapunov equation (Eq. 4.3). L_i is the Lagrange multiplier obtained by treating the Lyapunov equation as a constraint equation.

In order to compare sensitivities taken with respect to parameters of different units, the normalized sensitivities are computed as follows.

$$\frac{\frac{\partial \sigma_{zi}}{\partial \omega}}{\frac{\sigma_{zinom}}{\omega_{nom}}} = \frac{\partial \sigma_{zi}}{\partial \omega} \cdot \frac{\omega_{nom}}{\sigma_{zinom}} \approx \frac{\Delta \sigma_{zi}}{\Delta \omega} \cdot \frac{\omega_{nom}}{\sigma_{zinom}} \quad (4.23)$$

$$\approx \frac{\% \text{ change in } \sigma_{zi}}{\% \text{ change in } \omega}$$

Results obtained for the modal sensitivity analysis of mirror are shown in Table 4.2-1. The first mode analytical sensitivity is -1.7308, which means if the first natural frequency of the mirror is increased by an amount of 1%, it will result in a 1.73% decrease in the performance RMS value.

Table 4.2-1. Modal parameter sensitivity analysis results of Torsional scanner. Analytic solution and finite difference solution techniques are compared

	Analytic Solution	Finite Difference
1 st mode sensitivity	-1.7308	-1.7286
2 nd mode sensitivity	-1.3786 e -5	-1.3766 e -5
3 rd mode sensitivity	-1.1561 e -6	-1.1544 e -6
4 th mode sensitivity	3.8074 e -15	0
5 th mode sensitivity	1.7141 e -16	0
6 th mode sensitivity	-1.8287 e -16	0

If Table 4.2-1 is observed carefully, it can be seen that the first mode's sensitivity is significantly larger than the others. Additionally second and third modes' sensitivities are close to each other and they are much larger than the fourth, fifth, and sixth modes. This is an expected result if we observe the transfer function plot that relates the mirror rotation output to the given torque disturbance input in Figure 4.2-1(a). The first mode of the scanner at 5578 Hz is very dominant so performance is very sensitive to this mode. From the transfer function plot, it can be seen that second and third modes are also dominating at higher frequencies and they both have similar gains. The same trend is observed for the 2nd and 3rd modes sensitivities in Table 4.2-1. The 4th, 5th and the 6th modes are not observed in the transfer function plot and their

sensitivities are close to zero. In figure 4.2-1 it is emphasized that three modes are very dominant compared with the others. These three can be observed also in Table 4.2-1.

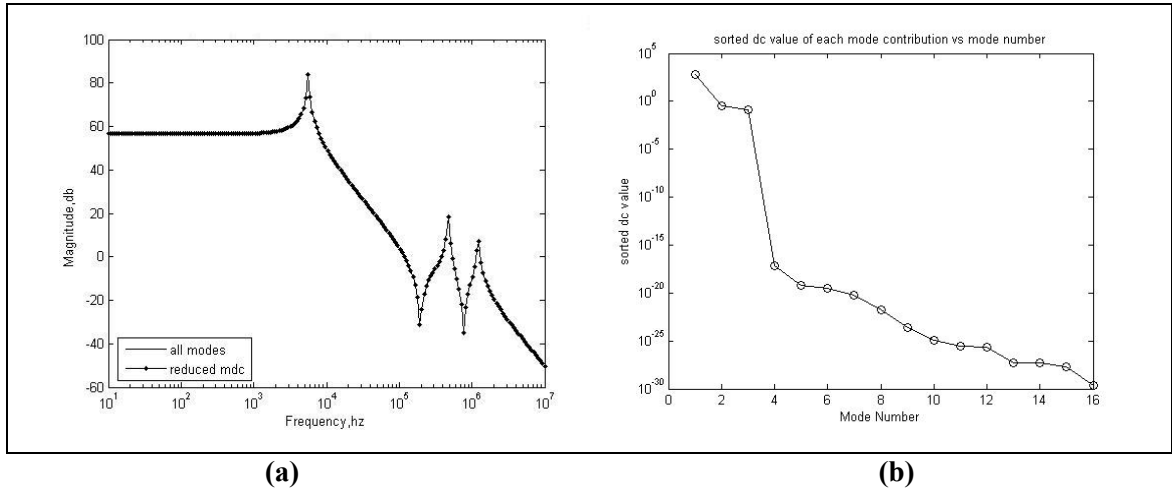


Figure 4.2-1 (a) The transfer function plot for the torsional scanner. Three modes can be observed while the others cannot. (b) the modes' dc gain values, however modes are sorted with respect to their dc gain contribution. Three modes having larger gains can be easily noticed among the others.

4.2.3 Modal Parameter Sensitivities Using Finite Difference Approach

Instead of computing the sensitivity exactly, another approach is to approximate the derivative with finite difference method. The finite difference technique is used in the modal and physical parameter sensitivity calculations as an alternative method to the exact solution.

In the modal parameter sensitivity analysis, the natural frequency value is perturbed, the Lyapunov equations are solved both for perturbed and unperturbed cases and the difference of the performances is calculated. The ratio of the difference of the two performances and the perturbed parameter's perturbation size gives the sensitivity value as an approximation.

$$\frac{\sigma_{zi} - \sigma_{zi \text{ perturbed}}}{\omega - \omega_{\text{perturbed}}} = \frac{\Delta \sigma_{zi}}{\Delta \omega} \quad (4.24)$$

Modal parameter sensitivities calculated by finite difference method are listed in Table 4.2-1. As it can be observed from the tabulated results, they all show good correlation between the finite difference and analytical values. The magnitude of the percent error between the finite

difference value and the exact value is shown as a function of perturbation size in Figure 4.2-2. The error in the sensitivities with respect to frequency decrease as the perturbation size becomes smaller. This is an expected result because the $\frac{\Delta\sigma_{zi}}{\Delta\omega}$ approximation to the derivative should approach the exact answer in the limit as $\Delta\omega$ approaches 0.

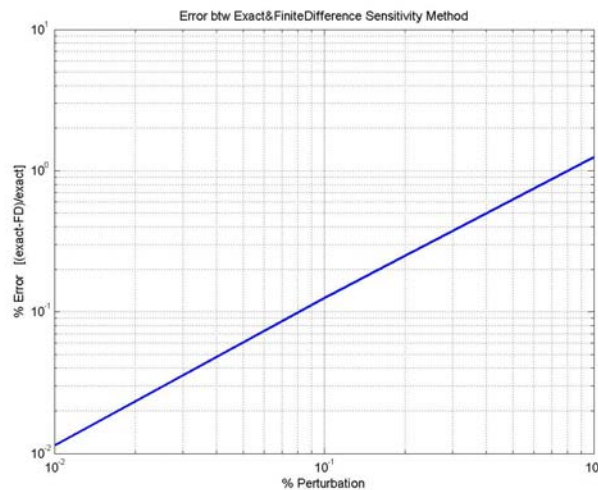


Figure 4.2-2: Variation of the error between finite difference method solutions and the exact solution with respect to the perturbation factor. The error of the finite difference method grows logarithmically with the increasing perturbation size.

4.2.4 Physical Parameter Sensitivities Using Analytical Approach

If the nominal design of a MEMS device fails to meet specified requirements, the physical parameters can be modified to improve the performance of the system. Especially for the systems with many design parameters, it is very difficult to identify the critical parameters that would affect the performance of the system. When the physical parameter sensitivity information is available it becomes easier to identify the areas for redesign.

If sensitivity is calculated with respect to a physical parameter p , it will not appear explicitly in the state-space matrices \mathbf{A}_{zd} , \mathbf{B}_{zd} and \mathbf{C}_{zd} . However the mode shapes in Φ , the modal frequencies in Ω and the modal masses in \mathbf{M} can depend on p . Thus the parameter dependence can be expressed in functional notations.

$$\begin{aligned}\mathbf{A}_{zd} &\rightarrow \mathbf{A}_{zd}(\Phi(p), \Omega(p), \mathbf{M}(p)) \\ \mathbf{C}_{zd} &\rightarrow \mathbf{C}_{zd}(\Phi(p))\end{aligned}\quad (4.25)$$

Then the derivatives of matrices \mathbf{A}_{zd} , \mathbf{C}_{zd} and their transposes need to be computed [16].

$$\frac{\partial \mathbf{A}_{zd}}{\partial p} = \sum_{j=1}^N \left(\frac{\partial \mathbf{A}_{zd}}{\partial \omega_j} \frac{\partial \omega_j}{\partial p} + \sum_{i=1}^n \frac{\partial \mathbf{A}_{zd}}{\partial \Phi_{ij}} \frac{\partial \Phi_{ij}}{\partial p} \right) \quad (4.26)$$

$$\frac{\partial \mathbf{C}_{zd}}{\partial p} = \sum_{j=1}^N \sum_{i=1}^n \left[\begin{array}{cc} \frac{\partial \mathbf{C}_{zd}}{\partial p} & 0 \\ \frac{\partial \Phi_{ij}}{\partial p} & 0 \end{array} \right] \frac{\partial \Phi_{ij}}{\partial p} \quad (4.27)$$

At this point, it is apparent that two types of derivatives are required. The first type is the derivative of state-space matrices with respect to modal parameters (frequencies, mode shapes and modal masses); the second type is the frequency, mode shape and modal mass derivatives with respect to physical parameters. These derivatives can be computed exactly using methods developed by Fox and Kapoor [6] and Nelson [8]. This is the reason for dividing the problem into two sections of modal and physical parameter sensitivities. The first type was studied in section 4.2.1 and the second type will be briefly discussed in this section.

The natural frequency and mode shape derivatives with respect to physical parameters can be generalized under the category of eigenvalue and eigenvector sensitivities. The eigenvalue derivative can be determined by first considering the familiar eigenvalue problem for a structural system, constructed as stiffness $[\mathbf{K}]$ and mass $[\mathbf{M}]$ matrices.

$$(-\omega_j^2 \mathbf{M} + \mathbf{K}) \phi_j = 0 \quad (4.28)$$

Differentiating the above eigenvalue problem and pre-multiplying each term by ϕ_j^T yields

$$\phi_j^T (-\omega_j^2 \mathbf{M} + \mathbf{K}) \frac{\partial \phi_j}{\partial p} + \phi_j^T \left(-\omega_j^2 \frac{\partial \mathbf{M}}{\partial p} + \frac{\partial \mathbf{K}}{\partial p} \right) \phi_j - \frac{\partial \omega_j^2}{\partial p} \phi_j^T \mathbf{M} \phi_j = 0 \quad (4.29)$$

In Eq. 4.29 the first addition term is the transpose of the initial eigenvalue problem and yields to zero, the last term includes a multiplication of a mode shape by its transpose which results in unity. So the derivative equation simplifies into

$$\frac{\partial \omega_j^2}{\partial p} = \phi_j^T \left(-\omega_j^2 \frac{\partial \mathbf{M}}{\partial p} + \frac{\partial \mathbf{K}}{\partial p} \right) \phi_j \quad (4.30)$$

As indicated in the above equation derivatives of mass and stiffness matrices with respect to physical parameter p need to be calculated in order to obtain the natural frequency derivative.

However computation of mode shape derivatives is a bit complicated. If (4.26) is differentiated but this time not pre-multiplied by ϕ_j^T the following equation is obtained

$$\left(-\omega_j^2 \mathbf{M} + \mathbf{K} \right) \frac{\partial \phi_j}{\partial p} = \frac{\partial \omega_j^2}{\partial p} \mathbf{M} \phi_j - \left(-\omega_j^2 \frac{\partial \mathbf{M}}{\partial p} + \frac{\partial \mathbf{K}}{\partial p} \right) \phi_j \quad (4.31)$$

As indicated in [14] the solution of the above equation is not possible with direct methods such as Gauss-Jordan elimination, therefore alternative solution techniques are required. First of all a solution in the form assumed

$$\frac{\partial \phi_j}{\partial p} = \psi_j + a \phi_j \quad (4.32)$$

As a summation of particular and homogenous solutions which are two perpendicular vectors.

Then another relation $\phi_j^T \mathbf{M} \phi_j = 1$ is differentiated with respect to p and the assumed solution is substituted, a solution for coefficient a can be obtained here as

$$a = \frac{1}{2} \phi_j^T \frac{\partial \mathbf{M}}{\partial p} \phi_j \quad (4.33)$$

In order to obtain the particular solution for ψ_j , another technique is suggested by Nelson [27]. Applying the Nelson's technique enables Eq. 4.29 to be solved using standard techniques.

Differentiating the above eigenvalue problem and obtaining the derivatives of mass and stiffness matrices with respect to physical parameter p need to be calculated in order to obtain the natural frequency derivative. One difficulty arises here since the stiffness and mass matrices are not very easy to obtain for larger order systems. Computation of mode shape derivatives is even

more complicated. In order to obtain the particular solution for $\frac{\partial \phi_j}{\partial p}$, a technique is suggested by Nelson. Applying the Nelson's technique enables the calculation of mode shape derivatives.

Considering the amount of computation time required to calculate the natural frequency and mode shape derivatives, and the difficulty of obtaining the stiffness and mass matrices, the analytical method is not found to be suitable for our sensitivity framework. Besides the stiffness and mass matrices are not easy to obtain for larger order systems especially when different types of elements are used in the finite element model. Considering all these drawbacks of the analytical approach, finite difference method is selected for the calculation of the physical parameter sensitivities of the torsional MEMS scanner.

4.2.5 A Benchmark Example for Physical Parameter Sensitivities Using Analytical Solution: Cantilever Beam Example

The derived equations are applied on a cantilever beam example for demonstration. The main reason for choosing a cantilever beam is the simplicity in calculating mass and stiffness matrices and their derivatives. Also the beam example is a single element model of a Bernoulli-Euler beam which has six degrees of freedom at each node that enables the calculation of the modes and mode shapes by hand. Finally, a beam is a 1D structure therefore it does not include any coordinate transformations. The stiffness and mass matrices of a Bernoulli-Euler beam are given. The derivative of these matrices can be easily obtained for the desired physical parameter.

$$\mathbf{K}_{\text{element}} = \begin{bmatrix} \frac{EA}{L} & 0 & 0 & 0 & 0 & 0 & -\frac{EA}{L} & 0 & 0 & 0 & 0 & 0 \\ 0 & \frac{12EI_z}{L^3} & 0 & 0 & 0 & \frac{6EI_z}{L^2} & 0 & -\frac{12EI_z}{L^3} & 0 & 0 & 0 & \frac{6EI_z}{L^2} \\ 0 & 0 & \frac{12EI_y}{L^3} & 0 & -\frac{6EI_y}{L^2} & 0 & 0 & 0 & -\frac{12EI_y}{L^3} & 0 & -\frac{6EI_y}{L^2} & 0 \\ 0 & 0 & 0 & \frac{GJ}{L} & 0 & 0 & 0 & 0 & 0 & -\frac{GJ}{L} & 0 & 0 \\ 0 & 0 & -\frac{6EI_y}{L^2} & 0 & \frac{4EI_y}{L} & 0 & 0 & 0 & \frac{6EI_y}{L^2} & 0 & \frac{2EI_y}{L} & 0 \\ 0 & \frac{6EI_z}{L^2} & 0 & 0 & 0 & \frac{4EI_z}{L} & 0 & -\frac{6EI_z}{L^2} & 0 & 0 & 0 & \frac{2EI_z}{L} \\ -\frac{EA}{L} & 0 & 0 & 0 & 0 & 0 & \frac{EA}{L} & 0 & 0 & 0 & 0 & 0 \\ 0 & -\frac{12EI_z}{L^3} & 0 & 0 & 0 & -\frac{6EI_z}{L^2} & 0 & \frac{12EI_z}{L^3} & 0 & 0 & 0 & -\frac{6EI_z}{L^2} \\ 0 & 0 & -\frac{12EI_y}{L^3} & 0 & \frac{6EI_y}{L^2} & 0 & 0 & 0 & \frac{12EI_y}{L^3} & 0 & \frac{6EI_y}{L^2} & 0 \\ 0 & 0 & 0 & -\frac{GJ}{L} & 0 & 0 & 0 & 0 & 0 & \frac{GJ}{L} & 0 & 0 \\ 0 & 0 & -\frac{6EI_y}{L^2} & 0 & \frac{2EI_y}{L} & 0 & 0 & 0 & \frac{6EI_y}{L^2} & 0 & \frac{4EI_y}{L} & 0 \\ 0 & \frac{6EI_z}{L^2} & 0 & 0 & 0 & \frac{2EI_z}{L} & 0 & -\frac{6EI_z}{L^2} & 0 & 0 & 0 & \frac{4EI_z}{L^2} \end{bmatrix} \quad (4.34)$$

$$\mathbf{M} = \frac{\rho AL}{420} \begin{bmatrix} 175 & 0 & 0 & 0 & 0 & 0 & 35 & 0 & 0 & 0 & 0 & 0 \\ 0 & 156 & 0 & 0 & 0 & 22L & 0 & 54 & 0 & 0 & 0 & -13L \\ 0 & 0 & 156 & 0 & -22L & 0 & 0 & 0 & 54 & 0 & 13L & 0 \\ 0 & 0 & 0 & \frac{105(I_y + I_z)}{A} & 0 & 0 & 0 & 0 & 0 & 0 & 0 & 0 \\ 0 & 0 & -22L & 0 & 4L^2 & 0 & 0 & 0 & -13L & 0 & -3L^2 & 0 \\ 0 & -22L & 0 & 0 & 0 & 4L^2 & 0 & 13L & 0 & 0 & 0 & -3L^2 \\ 35 & 0 & 0 & 0 & 0 & 0 & 175 & 0 & 0 & 0 & 0 & 0 \\ 0 & 54 & 0 & 0 & 0 & 13L & 0 & 156 & 0 & 0 & 0 & 22L \\ 0 & 0 & 54 & 0 & -13L & 0 & 0 & 0 & 156 & 0 & 22L & 0 \\ 0 & 0 & 0 & 0 & 0 & 0 & 0 & 0 & 0 & \frac{105(I_y + I_z)}{A} & 0 & 0 \\ 0 & 0 & 13L & 0 & -3L^2 & 0 & 0 & 0 & 22L & 0 & 4L^2 & 0 \\ 0 & -13L & 0 & 0 & 0 & -3L^2 & 0 & -22L & 0 & 0 & 0 & 4L^2 \end{bmatrix} \quad (4.35)$$

Since the example is a single element cantilever beam, the stiffness and mass matrices can be reduced to 6x6 matrices (fixed end stiffness and mass components can be eliminated) and calculation becomes easier. For a system different than a cantilever beam, the stiffness and mass matrices are not so straightforward to obtain. Also different element types bring different directional orientations and need to be connected properly. Considering these drawbacks the analytical solution does not appear to be an appropriate method for sensitivity calculations.

The derivative term $\frac{\partial \omega_j^2}{\partial p}$ in Eq. 4.28 can be calculated using the mass and stiffness matrices given in Eq. 4.34 and 4.35. The eigenvector derivative $\frac{\partial \phi_j}{\partial p}$ cannot be obtained directly; as a result Nelson's method is used.

The achieved results are then compared with a finite difference solution. It is observed that results obtained by finite difference approach match well with the analytical solution.

4.2.6 Physical Parameter Sensitivities Using Finite Difference Approach

The finite difference solution technique for the physical parameters' sensitivities is similar to the modal parameters' sensitivities. The physical parameters are perturbed one at a time in the finite element analysis, the state space model is reconstructed for the perturbed system, and the

performance is calculated using the Lyapunov approach. The performance difference between the perturbed system and the original system is then divided by the perturbed parameter step size and the sensitivity value is approximated. The same example demonstrated in section 4.2.3 is solved again with finite difference approach and it is found that the method also works well. The analytic solution and finite difference solutions of the beam example are compared in Figure 4.2-3, and it is found that they match well with each other.

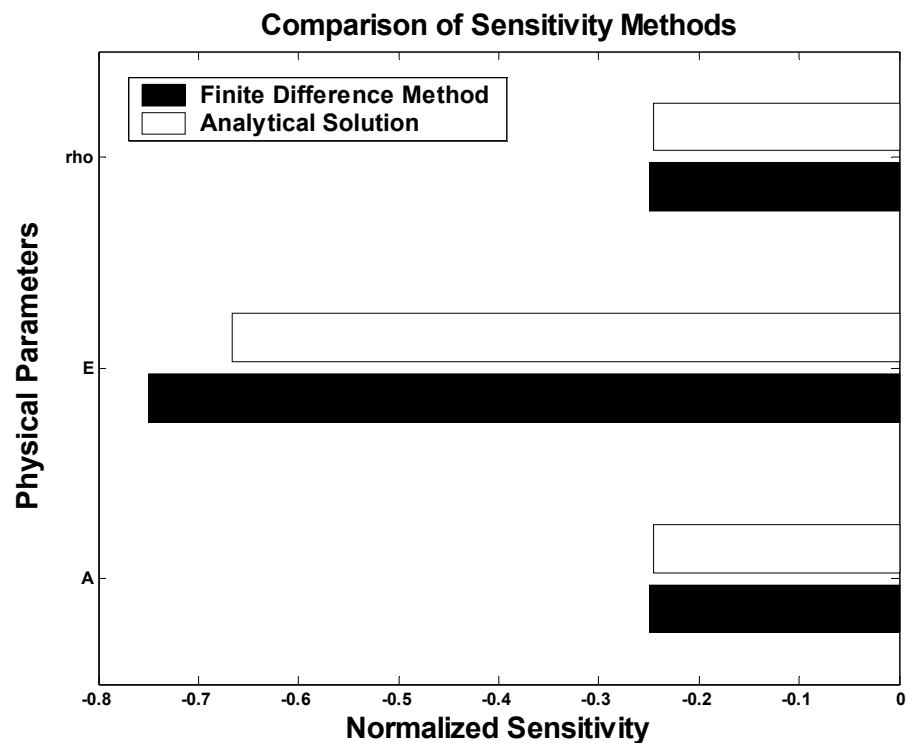


Figure 4.2-3: Comparison of two different sensitivity analysis methods, applied on a cantilever beam. The physical parameters, which sensitivities are calculated with respect to are ‘A’ beam cross sectional area, ‘E’ elastic modulus, and ‘ ρ ’ the density of the beam material.

4.2.7 Sensitivity Analysis of a Microscanner

The microscanner model shown in Figure 4.1-1 is analyzed for its parameters’ sensitivities. The box shaped flexures of the scanner are the main design variables when the stiffness of the system is considered. We performed the physical sensitivity analysis on the design variables shown in Figure 4.1-1 using the finite difference approach (see section 4.2.2 for details). Table 4.2-2 tabulates the physical parameter sensitivities for the torsional MEMS scanner.

Table 4.2-2. Physical parameter sensitivity analysis of the torsional MEMS scanner.

	Computed Normalized Sensitivity
Flexure Width (w)	-1.507
Flexure Thickness (t)	-1.507
Flexure Length (L)	0.7549
Elastic Modulus (E)	-0.7540
Density (ρ)	-0.2398
Mirror Thickness (t_m)	-0.2398
Mirror Width (w_m)	-0.5990
Mirror Height (h_m)	-0.3596

Among the computed sensitivities, the greatest sensitivity belongs to the flexure beam width and thickness. A 1% increase in the flexure width or thickness will result in 1.507% decrease in the RMS performance value. Since the performance is defined as the deviation of the mirror tilt angle under random disturbances, increasing the beam thickness or width results in an increase in system stiffness and a decrease in this deviation. For the flexure beam length, it is the adverse effect. Increasing the flexure length by 1% results in an increase at the performance by an amount of 0.755%. The flexure parameters such as width and thickness are suitable for redesign however changing the length of the flexure may not always be possible due to spacing problems. The mirror dimensions are directly related to optical resolution of the system so they are not generally included in the structural redesign efforts. However, the sensitivity results show that they are as significant as the flexure dimensions in terms of determining the performance of the torsional scanner.

4.3 Design Procedure

The analysis steps may be employed from the beginning to the end of a certain design to predict the performance of the design and change it if necessary. These schematic of these are shown below in figure 4.3-1.

The procedure begins with FEM of the newly designed structure. A detailed model can be used as well as a simplified model as long as it represents the real system dynamics.

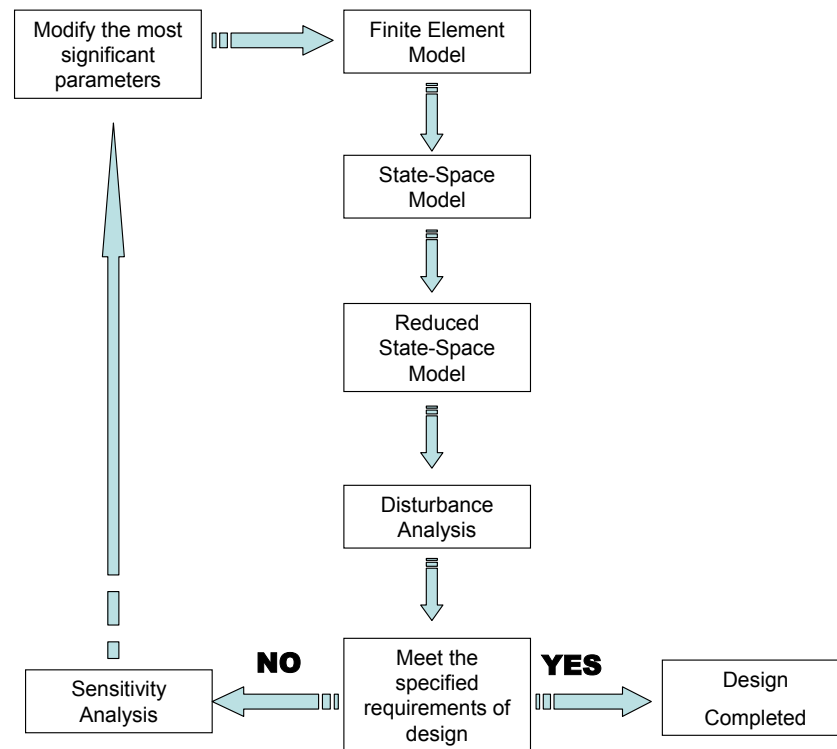


Figure 4.3-1: The schematic of the design procedure with performance prediction and sensitivity analysis.

The modal analysis is conducted with the FEM and the results are output to text files. The performance should be determined at this step, because only the directions related with the performance definition are going to be extracted from modal analysis solutions. The state-space representation is constructed using the FEM modal analysis results. Since the model is ready now, further analysis for performance prediction may be applied. The design is successful, if the performance of the design meets the specified requirements. However, redesign is necessary if it fails. In order to concentrate the redesign efforts on the correct parameters, the sensitivity analysis should be conducted. It is possible to identify the critical parameters of the system with sensitivity analysis. A new design is build by changing the identified parameters, the FEM must be created for this design and analysis steps should be employed from the beginning. This procedure can be applied as a loop for a performance optimization routine.

Chapter 5

EXPERIMENTAL STUDY

5.1 Introduction

Any unwanted effect that is coming from the environment or from the equipment used can be considered as disturbance, in that it potentially interferes with the accuracy of the desired output. Development of a disturbance framework requires the real time disturbance inputs to be measured and to be modeled as precise as possible. The disturbance shaping filter, introduced in Chapter 3, is constructed using the measured disturbances. Measurement of the disturbance is a complicated process, since disturbances are never desired system inputs and there are no tools for direct measurement of the environmental disturbances. This chapter summarizes the procedure and the techniques that we developed to calculate the disturbances acting on the microscanners. The following section describes the equipment used in the experiments. The details of the procedure and the results are presented in Sections 5.3 and 5.4.

5.2 Equipment

The experimental equipment is provided by Optical Microsystems Laboratory and Mechanical Vibrations and Design Laboratories at KOÇ University. The microscanner used is a product of Microvision Company, with its self testing board. A function generator is used to create the drive signal for the microscanner. The fundamental measurement device is a Polytec Laser Doppler Vibrometer (LDV), which is placed directly across the scanner surface. LDV readings can be seen from an oscilloscope or data can be transferred to a PC and processed, using a data acquisition card and suitable software, such as Labview. The Labview program created and used during the measurements is shown in Figure 5.2-1.

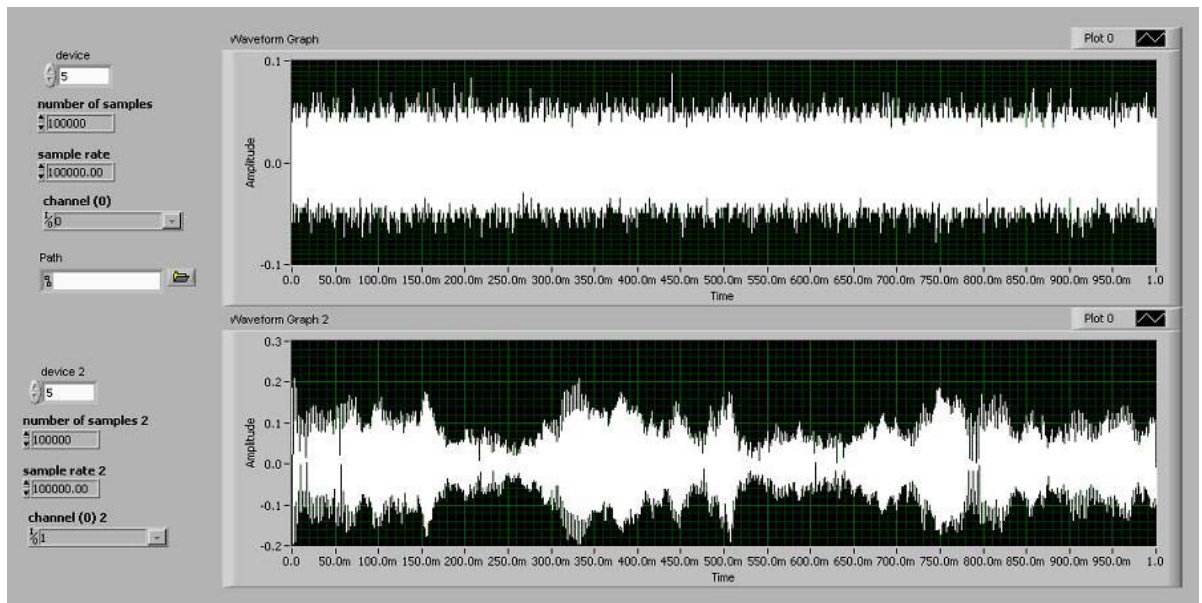


Figure 5.2-1: The LABView screen shot. The program is constructed in order to measure the disturbances.

5.2.1 Microscanner

In the experimental study, disturbances on a biaxial scanner are measured. The scanner is a product of Microvision Company. The scanner chip is attached to a carrier printed circuit board (PCB) which is a part of a standard MEMS test system at Microvision. This is shown in Figure 5.2-2. The test system consists of drive circuitry for the horizontal and vertical axes, as well as an optical mounting interface. Onboard phase control circuitry provides analog closed loop operation of the part. A ZIF socket allows easy part changes [28]. This is a biaxial scanner with horizontal, fast scan and vertical, slow scan axes. These two main moving frames, whose motion axes are perpendicular to each other, enable the scanner to create a 2D image or scan a 2D area with the reflected light beam. The scanner that was modeled in the previous chapters, is a single axial scanner. We used a 2D scanner instead since the 1D scanner was not available at the time of the experiments. The characterization of the disturbances for both scanners are the same since they measured in the same environment.

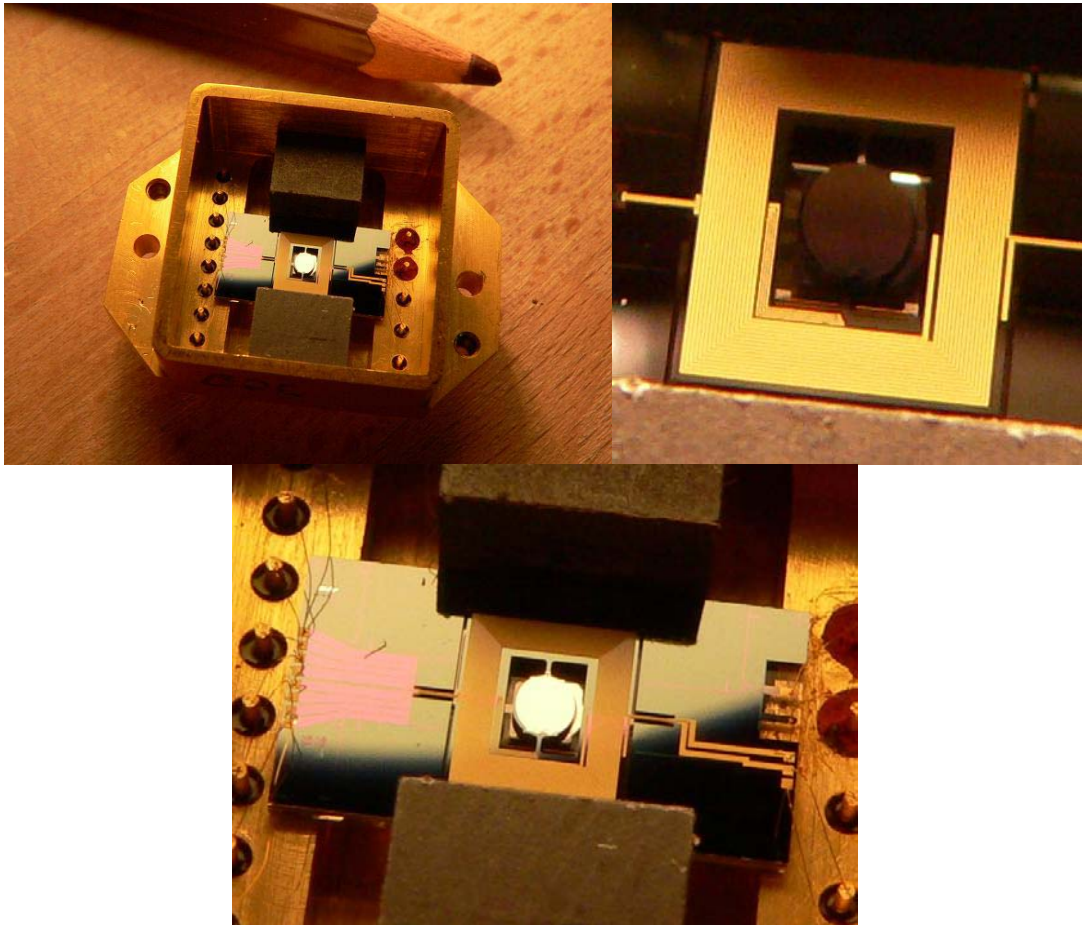


Figure 5.2-2: Microvision Biaxial MEMS scanner. First picture showing the scanner in the casing with the permanent magnets, below this picture coils used to drive the scanner can be seen on the outer frame. The third one is a close up picture, slow scan and fast scan frames and flexures can be identified.

The microscanner is electro-magnetically actuated. The permanent magnets on the sides create a constant magnetic field. When a current is passed through the coils on the moving plate, an in-plane electromagnetic force is exerted on the mirror, which leads to torsional deflection. This force is proportional to the magnetic field intensity, the current passing through the conductor and the length of the conductor inside the magnetic field.

5.2.2 Piezoresistive Sensors

The flexures of the moving frames are coated with a layer of piezoresistive material, for position sensing. Piezoresistivity is the dependence of electrical resistivity on strain. The resistivity of

the material depends on the internal atom positions and their motions. Strains change these arrangements and, hence, the resistivity [29]. Piezoresistive layers enable the sensing of the strain and position. The test board of the scanner facilitates data acquisition from these sensors to an oscilloscope or a data acquisition system. However, piezoresistive sensors measure voltage due to strain and angular displacement where LDV measures translational velocity. Therefore a conversion factor is necessary to obtain correct angular position data from piezoresistive sensors'. The scaling factor between the voltage output and actual rotation can be found as described in figure 5.2-3.

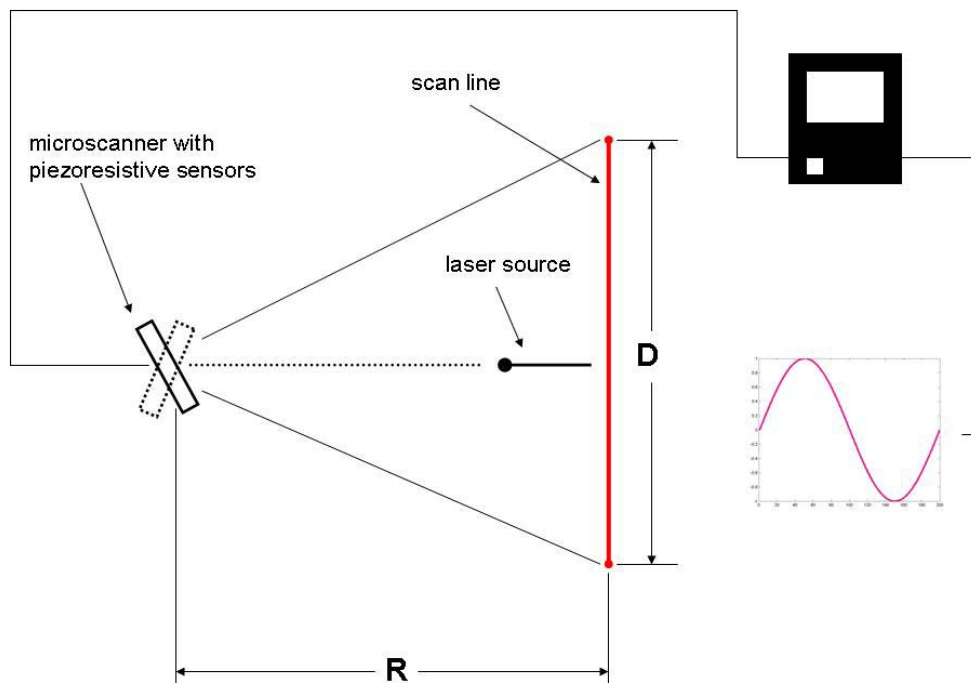


Figure 5.2-3: the schematic showing the setup for piezoresistive sensor readings. The sensors can be directly connected to an oscilloscope or a pc with a data acquisition system.

R is screen mirror distance and D is the measured scan line. The length of the scan line can be easily measured and the corresponding peak to peak voltage (V_{pp}) value of piezoresistive sensors can be read from the oscilloscope. Using basic geometric relations, the angular position can be easily calculated using the measure voltage.

$$\theta = \tan^{-1}\left(\frac{D/2}{R}\right) \quad (5.1)$$

$$\text{conversion factor} = \frac{\theta}{V_{pp}} \quad (5.2)$$

5.2.3 Laser Doppler Vibrometer

A Laser Doppler Vibrometer (LDV) is a device that measures the velocity of a moving particle using the Doppler Effect. Doppler Effect is the phenomenon of the wavelength shift of the light due to the moving light source. In the case of LDV, the light beam is reflected from a moving surface, this also results a shift in the wavelength of the light which is then used to calculate the velocity of the moving object.

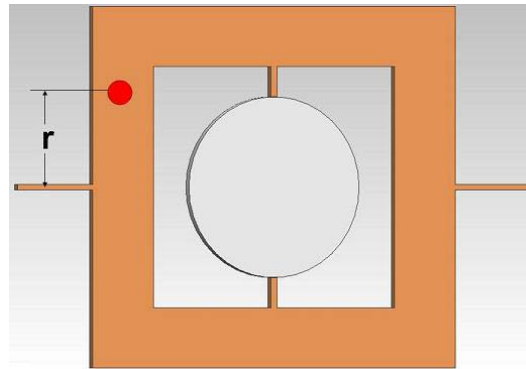


Figure 5.2-4: LDV measurement point, for the torsional mode of the outer frame.

LDV is measuring the translational velocity of a point. The desired output is the angular position of the outer frame. The angular velocity of the outer frame can be calculated using the following equation.

$$V = r \times \omega \quad (5.3)$$

V is the translational velocity of the point which is read by LDV, ω is the angular velocity of the outer frame, and r is the distance between the spot and the frame rotation axis. Eq 5.3 is only valid when small angle assumption is made as it is demonstrated in Figure 5.2-5. The distance between the location of the spot and the rotation axis is equal to a constant 'r' if and only if $\cos \theta \cong 1$.

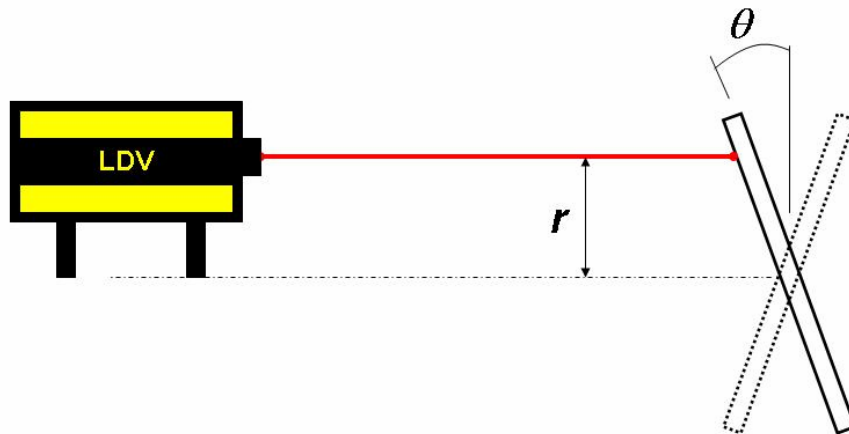


Figure 5.2-5: Schematic view of the LDV measurement setup, for the description of “small angle θ ” assumption.

5.3 Procedure

The experimental procedure (see Fig.5.3-1) that we developed starts with measuring the translational velocity using LDV and measuring the angular position using the piezoresistive sensors. Piezosensors and LDV data can be collected simultaneously. Piezoresistive sensor data was polluted with a lot of noise and it showed a stairway like behavior so it was not used for further analysis.

Angular velocity of the outer frame is calculated using Eqn. 5.3 utilizing the translational velocity measured by LDV. The next step is integrating the velocity data in order to obtain the position. The sampling rate and sampling time are important parameters for the integration. 100,000 samples per second is the sampling rate while 0.1 is the sampling time. Integration for position is nothing but summing the displacements over the sampling time domain (Eq 5.4).

$$\theta_{\text{int}} = \sum \omega . dt \quad (5.4)$$

As we had explained at the beginning, any variation from the ideal output is generated by the disturbances acting on the system. If we subtract the “ideal” from the “measured”, that should give us the variation in the angular position. A low-pass filter was used to filter the high frequency signals from the measured data. The filtered data is called the ‘ideal’ case. Eqn. 5.5 is used to calculate the torque variance. Torque intensity used in the disturbance filter is calculated using the relation in Eqn. 5.6.

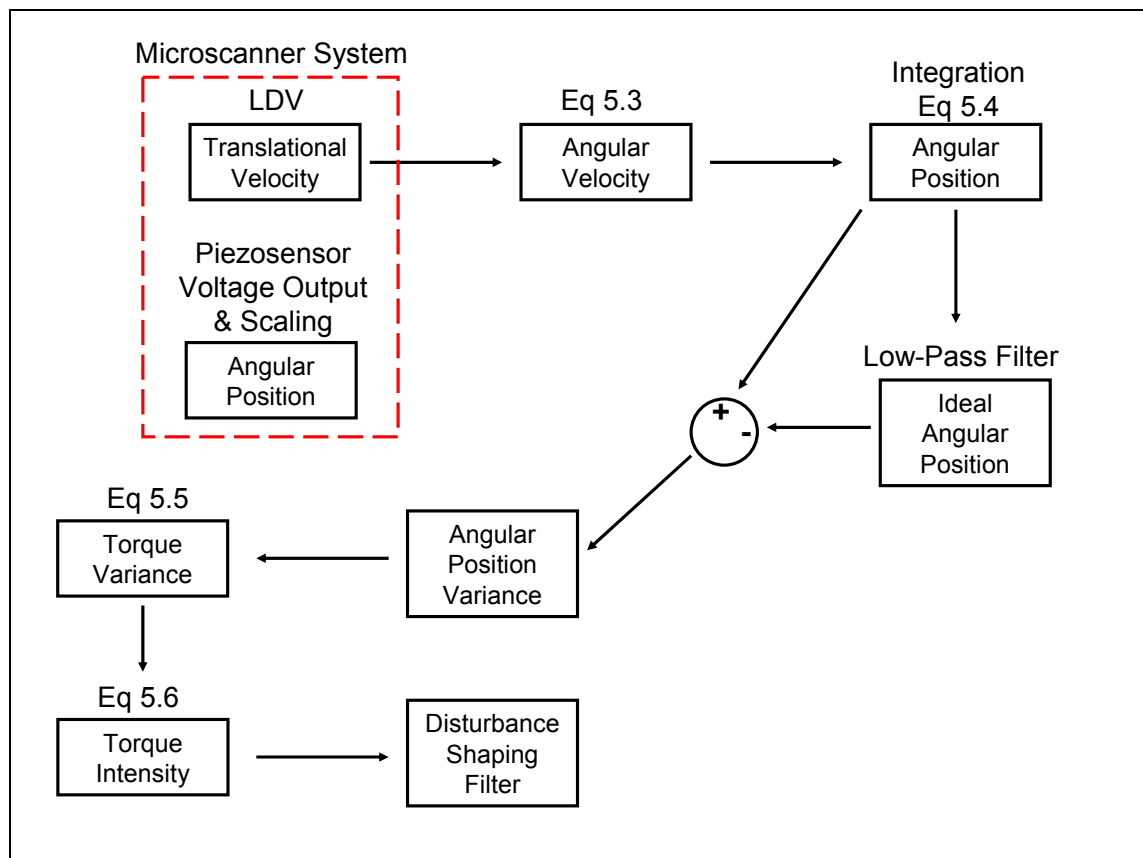


Figure 5.3-1: Schematic of disturbance measurement procedure.

5.4 Results

Direct position data from piezoresistive sensors and velocity data from LDV are gathered and analyzed.

5.4.1 Piezoresistive Sensors and Position Measurements

The first set of data that was collected with piezoresistive sensors. The data contains too much sensor noise, electrical noise, and electronic jitter. Also it has got a stairway like behavior due to the discrete sampling time nature of the sensor.

The piezoresistive sensor data is taken into MATLAB, and filtered with a low-pass filter to reduce the effect of the noise on the signal.

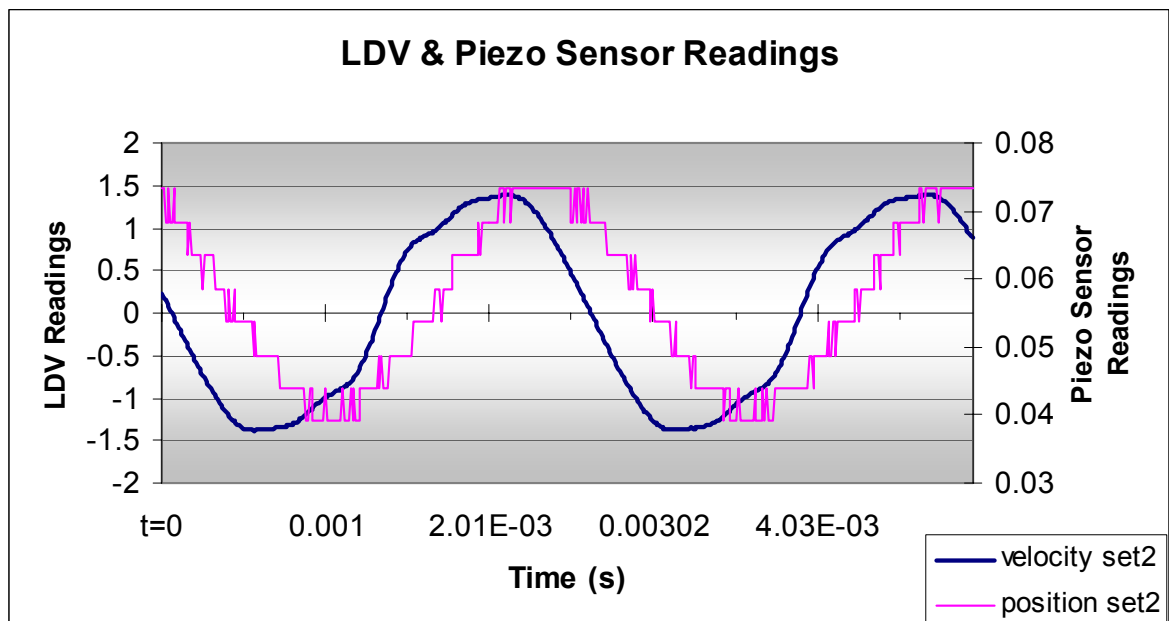


Figure 5.4-1: LDV Readings versus Piezoresistive Sensor readings. (The noise on the piezoresistive sensor data can be seen easily)

5.4.2 LDV and Velocity Measurements

The LDV readings are more smoother compared with the piezoresistive sensor readings, therefore they are used to calculate the disturbances. Besides LDV can measure small oscillations of velocity which results significant position deviations.

When two data sets are compared, in figure 5.4-1, a certain phase difference can be observed. The phase difference should be 90° , considering the fact that one is position data and the other is the velocity. However the different electronic circuits behind these two independent systems create their own internal delay times, and these delays are completely independent of each other. Therefore the observed phase difference between the position and velocity is not always 90° . the velocity data is integrated to get the position data. As it can be seen from Figure 5.4-4 the phase difference disappears. Note that the units in Figure 5.4-3 and 5.4-4 do not reflect the real velocity and position values.

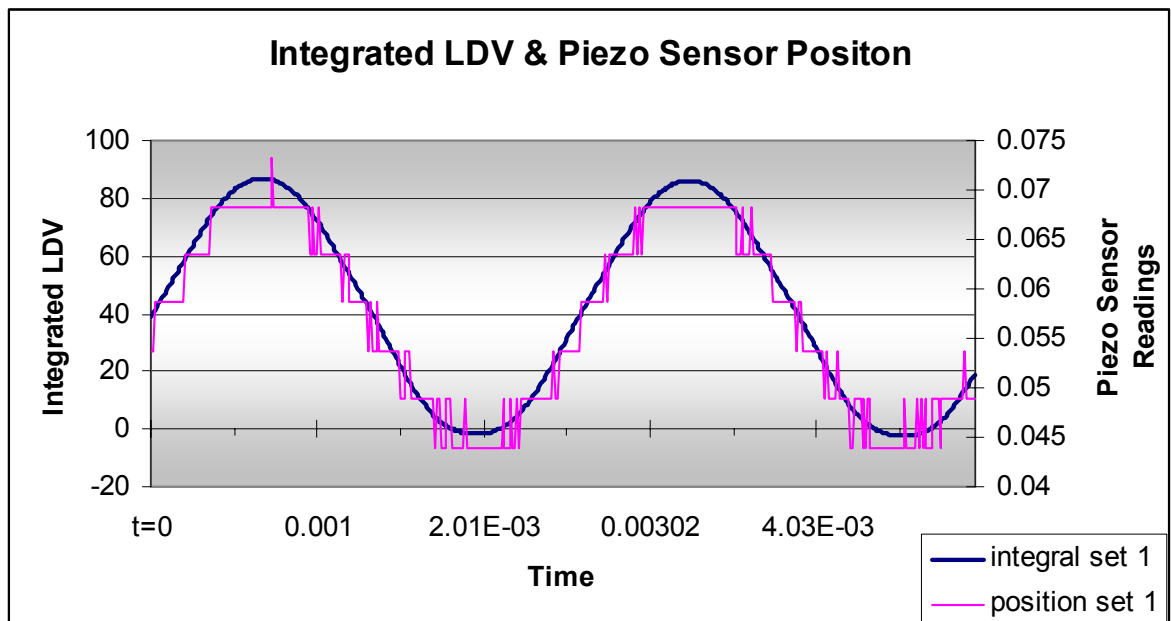


Figure 5.4-2: The position obtained by integration of the velocity and obtained from piezoresistive sensors. The left hand side y- axis represents the integrated LDV results for position, while the right hand side represents piezoresistive sensor outputs.

As it was explained in Section 5.3 the difference between the ‘measured’ position and the ‘ideal’ position occurs due to disturbances acting on the mirror. We applied some smoothing algorithms, to filter the measured data and generate an ‘ideal’ case. These signals are shown in the Figure 5.4-3. Figure 5.4-4 represents the difference between those two signals.

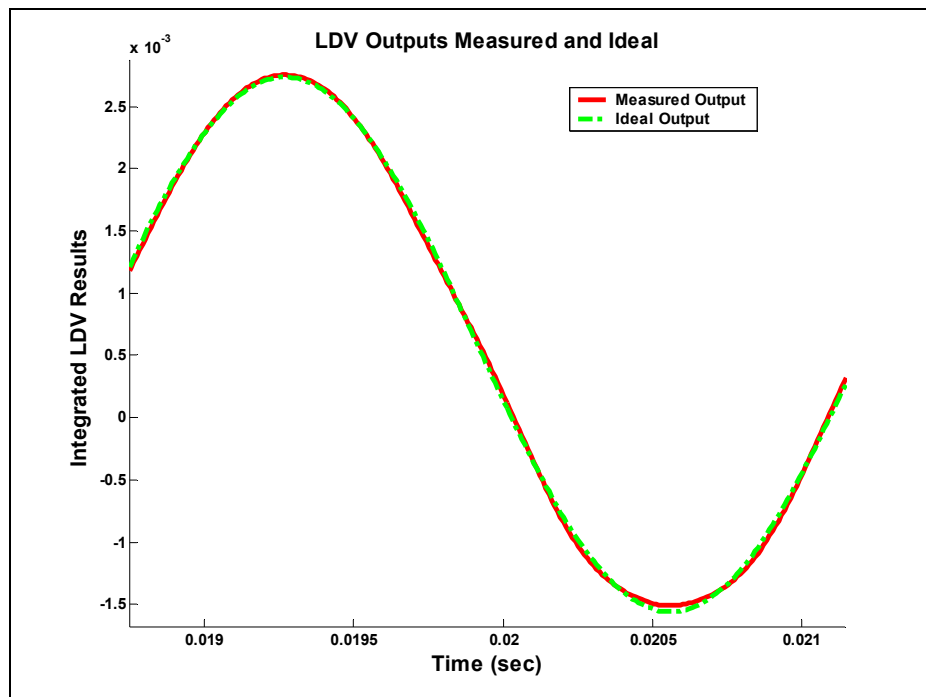


Figure 5-4-3: Ideal and measured position data. The measured data seems to fit with the ideal one, however there occurs a little difference which is enough for disturbance calculations.

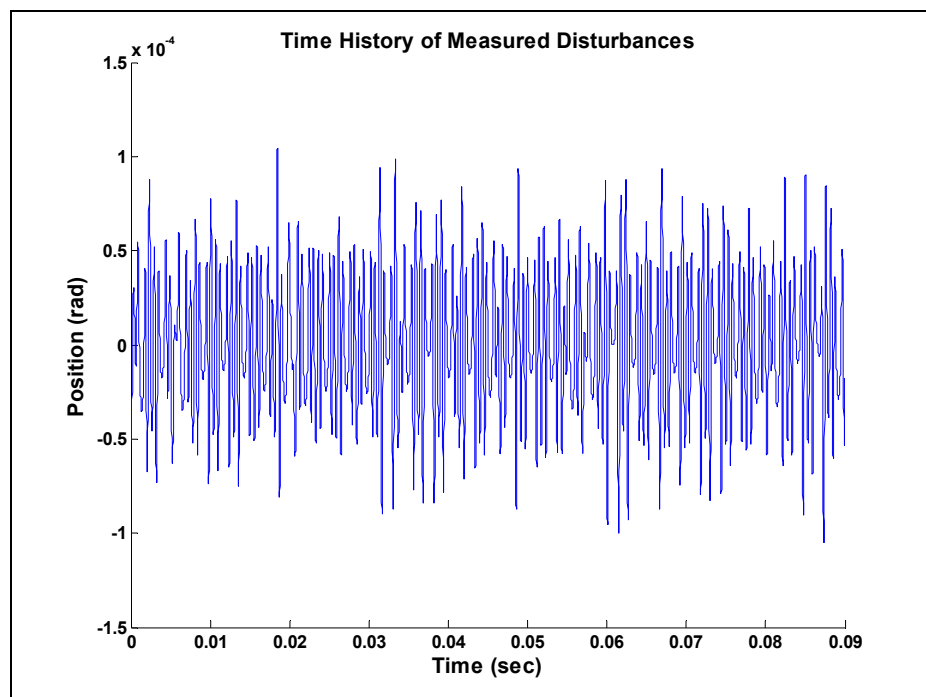


Figure 5.4-4: The time history for the disturbances, the difference between the measured and the ideal. RMS values for the measured disturbance is calculated as 3.6×10^{-5}

5.4.3 Torque Intensity

The disturbance analysis tool, based on the Lyapunov approach, is derived for ‘unit intensity white noise’, and this unit intensity must be modified with the real disturbance intensity.

The variation of the position is (see Figure 5.4-6) is plugged into the following equation to obtain the disturbance torque.

$$J_{eff} \ddot{\theta} + b\dot{\theta} + k_{tors} \theta = T_{dist} \quad (5.5)$$

The inertia, damping and stiffness properties are calculated using the same formulas that was introduced in section 3.4. Figure 5.4-7 demonstrates the disturbance torque calculated using Eq. 5.5. The disturbance noise intensity is defined in [30] as

$$D = \max[\Phi(\omega)] \quad (5.6)$$

where $\Phi(\omega)$ is the frequency dependent power spectrum of zero-mean disturbance. The intensity of the disturbance is calculated using the above formula.

The disturbance intensity for the input torque is calculated as 1.75×10^{-12} Nm. The calculated disturbance intensity is used as the disturbance magnitude input for the disturbance analysis toolbox.

Chapter 6

DISCUSSION AND CONCLUSION

In this thesis, we have developed an integrated design approach that incorporates modeling and analysis tools for analyzing system performance, sensitivity of design parameters and critical components of MEMS devices. We demonstrated the use of the developed methodology through a case study which includes the disturbance and sensitivity analysis of a MEMS scanner mirror.

The MEMS scanner mirror is modeled using the commercial FEM software , ANSYS. Modal analysis module of ANSYS was used to obtain the mode shapes and natural frequencies of the system. As described in Chapter 2, two models were generated. One of them was with solid elements and the other one with ‘shell and beam’ elements. The solid model is reduced from 21294 degrees of freedom to 6930 degrees of freedom by modeling with ‘shell and beam’ elements. The modal analysis’ calculation time is significantly less for ‘shell and beam element model’ compared to ‘solid element model’. The main reason for less calculation time is the smaller number of elements and nodes for ‘shell and beam’ element model. We did not lose any accuracy in our predictions by reducing the fidelity since the mode shapes and natural frequencies of these two models matched quite well. Another advantage of using a simplified model is that, ‘shell and beam’ elements have rotational degrees of freedom in three mutually perpendicular axes. On contrary, solid elements have only translational freedoms at their nodes. Besides, the performance of the system is defined as the rotation of the mirror, which corresponds to the rotational degree of freedom about flexure axis (x- axis) in FEM. As a result, using an accurate simple ‘shell and beam model’ of the micro scanner is advantageous over the ‘solid element model’.

The FEM results were then transferred to MATLAB in order to build the state model of the mirror. The state-space form is one of the commonly used mathematical representations of a dynamical system. The state-space representation provides an easy way to solve second order differential equations and it is a very efficient way to investigate the input and output relations for transfer functions. Inputs are defined as torque disturbances acting on the mirror and

outputs are the amount of variance about the mirror rotation axis. This variance should be kept as small as possible in order to improve the performance of the scanner mirror.

Disturbance analysis and sensitivity analysis with Lyapunov approach takes great amount of time if large scale systems are used. Therefore, some model reduction techniques are performed to reduce the size of the FEM. These techniques were discussed in detail in Chapter 2. The applied algorithms aim to eliminate the insignificant states for the transfer functions of interest. For the scanner mirror example, the “dc gain” and “peak gain” approach worked really well. The reduced model transfer functions obtained by the “dc gain” and “peak gain” technique matched really well with the unreduced model. The reduced model is used in the performance prediction and sensitivity analysis studies..

A methodology was developed to predict the performance of a MEMS scanner mirror under random disturbance sources. The methodology uses Lyapunov equations in disturbance analysis and calculates the RMS value of the angular displacement which defines the performance of the scanning mirror. The results are compared with the time domain simulation of the same mirror modeled as a lumped mass-spring and damper system. The Lyapunov approach is found to be a very efficient and accurate method. Disturbance analysis is also required for the sensitivity analysis framework. Few drawbacks of this approach are; it may take too much time to solve the Lyapunov equations for large order systems and the solution does not provide any frequency insight for the variances. In other words, the frequency dependency of the performance is not observable from the results.

Sensitivity analysis framework is built on the disturbance analysis framework. First, the exact modal parameter sensitivities are calculated and validated with the results of the finite difference method. Modal parameter sensitivities are able to identify which modes are the most important however they do not provide any information regarding what physical characteristics of the design should be modified to affect the modes and improve the design. The analytical formulations for the physical parameter sensitivities are discussed and demonstrated, on the other hand, due to the complexity and the computational time required performing these calculations, they are not found to be suitable for the application of interest. Instead, the finite difference method is used to calculate the physical parameter sensitivities and concluded that the flexure dimensions play an important role in determining the performance of the mirror.

Sensitivity analysis tool is an extremely valuable tool especially when the MEMS system has many design parameters. One can easily identify the most significant design parameters that may effect the performance of the system using the methodology developed in this thesis. Then the designer can focus on these parameters to improve the performance.

The disturbances used in the disturbance analysis framework are obtained experimentally. An experimental set-up was built to measure the disturbances on the scanner mirror. The set-up includes an LDV that measures the translational velocity and a piezoresistive-sensor that measures the angular position of the mirror. LDV data was found to be much noiseless than the Piezoresistive sensor data. A methodology was developed to calculate the magnitude level of the disturbances acting on the system. The procedure to calculate the torque intensity in the disturbance shaping filter is explained in detail in Chapter 5.

This thesis summarizes our initial attempt to create a design and analysis tool for MEMS devices. The disturbance analysis framework provides the means for predicting the performance of such systems in a very efficient and accurate way. The sensitivity analysis framework is very valuable for diagnosing the problematic components that degrade the overall system performance. All the governing equations are written in MATLAB code which provides any easy way for further additions to the design tool. An automated routine was developed to generate state space model from the results of the finite element model. This routine can be applied to other MEMS devices to perform disturbance and sensitivity analysis. The Sensitivity analysis framework can be extended and then be used to perform a simultaneous optimization routine. In this study, we investigated the disturbances only for scanner mirrors. Since most of these disturbances are sensor and electronics dependent, other MEMS devices must be also studied to obtain various disturbance models.

REFERENCES

- [1] J. V. Clark, N. Zhou and K. S. J. Pister “MEMS Simulation Using SUGAR v0.5”
- [2] ANSYS Release 8.1 Documentation
- [3] FEMLAB, Users Manual.
- [4] H. Li and E. K. Antonsson “Evolutionary Techniques in MEMS Synthesis” September 1998 ASME Design Engineering Technical Conferences.
- [5] T. Mukherjee and G. K. Fedder, “Structured design of microelectromechanical systems,” *Proceedings of 34th ACM DesignN*.
- [6] Zhou, A. Agogino, and K. S. J. Pister, “Automated design synthesis for Micro-Electro-Mechanical Systems (MEMS),” *Proceedings of the ASME Design Engineering Technical Conference*,
- [7] H. Urey, “MEMS Scanners for Display and Imaging Applications,” submitted to *Photonics East*, 2004.
- [8] H. Urey, “Retinal Scanning Displays”, *Encyc. of Optical Engineering*, Marcel-Dekker, 2003.
- [9] Wolter, H. Schenk, E. Gaumont, H. Lakner, “MEMS microscanning mirror for barcode reading: from development to production,” *SPIE Proc. of MOEMS Display and Imaging Systems II*, vol. 5348, pp. 32-39, 2004.
- [10] H. Schenk, U. Dauderstädt, P. Dürr, A. Gehner, A. Wolter, H. Lakner, “Light processing with electrostatically driven micro scanning mirrors and micro mirror arrays,” *SPIE Proc. of MOEMS Display and Imaging Systems II*, vol. 5348, pp. 32-39, 2004.

- [11] H. Toshiyoshi, H. Fujita, "An electrostatically operated torsion mirror for optical switching device," *Proceedings of the 1995 Int. Conf. on Solid-State Sensors and Actuators (Transducer '99)*, vol. 68-B1, p. 199-200, 1995.
- [13] F. Shi, P. Ramesh and S. Mukherjee "Simulation methods for micro-electro-mechanical structures (MEMS) with application to a microtweezer" *Comput. Struct. (USA)*. Vol. 56, no. 5, pp. 769-783. 3 Sept. 1995
- [14] M. Allen, M. Rauli, K. Maute, D. M. Frangopol "Reliability-based analysis and design optimization of electrostatically actuated MEMS" *Comput. Struct.* Vol. 82, no. 13-14, pp. 1007-1020. May 2004
- [15] O. Sigmund "Design of multiphysics actuators using topology optimization – Part I: One material structures" *Computer Methods in Applied Mechanics and Engineering*, Volume 190, Number 49, 12 October 2001, pp. 6577-6604(28)
- [16] H. L. Gutierrez and D. W. Miller "Performance Assessment and Enhancement of Precision Controlled Structures During Conceptual Design", February 1999
- [17] Shabana, *Theory of Vibration*, vol. 2, Springer-Verlag, 1991.
- [18] Kan, H. Urey, C. Ataman "Dynamic modeling of comb-driven torsional scanners" submitted to Optical MEMS 2004, Kanagawa, Japan, August 2004
- [19] M. R. Hatch and B. Raton, "Vibration Simulation Using MATLAB and ANSYS" Chapman & Hall CRC c2001.
- [20] C. Ataman, "Design, Modeling and Characterization of Electrostatically Actuated Microscanners", September 2004
- [21] Z. Gaji'c and M. T. J. Qureshi , "Lyapunov Matrix Equation in System Stability and Control". San Diego : Academic Press, c1995.

-
- [22] K. Ogata, "Modern Control Engineering", Third Edition, Prentice Hall International, Inc. 1997
- [23] H. Urey, C. Kan W. O. Davis, "Vibration Mode Frequency Formulas for Micromechanical Scanners" *J. Micromech. Microeng.* 15 No 9 (September 2005) 1713-1721
- [24] R. G. Brown and P. Y. C. Hwang, "Introduction to Random Signals and Applied Kalman Filtering", John Wiley & Sons, Inc., 1997.
- [25] Ertas, J. C. Jones "The Engineering Design Process" New York : Wiley, c1993.
- [26] R. L. Fox and M. P. Kapoor, "Rates of Change of Eigenvalues and Eigenvectors", *AIAA Journal*, 6 (1968), pp. 2426-2429.
- [27] R. B. Nelson, "Simplified calculations of eigenvector derivatives", *AIAA Journal*, 14 (1976), pp. 1201-1205.
- [28] D. W. Wine, M. P. Helsel, L. Jenkins, H. Urey, T. D. Osborn, "Performance of a Biaxial MEMS-Based Scanner for Microdisplay Applications"
- [29] S. D. Senturia, "Microsystem Design", Kluwer Academic Publishers, 2001
- [30] M. M. Millonas, "Transport and current reversal in stochastically driven ratchets", arXiv:cond-mat/9401046 v1 21 Jan 1994
- [31] R. Sprague, T. Montague D. Brown, "Bi-axial magnetic drive for Scanned Beam Display mirrors"

PUBLICATIONS

F. C. Meral, I. Basdogan “Dynamic Analysis of a Torsional MEMS Scanner Mirror, Part 1: Disturbance Analysis Framework” Proceedings of IDETC/CIE 2005 ASME 2005 International Design Engineering Technical Conferences & Computers and Information in Engineering Conference September 24-28, 2005, Long Beach, California, USA

F. C. Meral, I. Basdogan “Dynamic Analysis of a Torsional MEMS Scanner Mirror, Part 2: Sensitivity Analysis Framework” Proceedings of IDETC/CIE 2005 ASME 2005 International Design Engineering Technical Conferences & Computers and Information in Engineering Conference September 24-28, 2005, Long Beach, California, USA

VITA

Faik Can Meral was born in Ankara Turkey, in 1981. He received his B.Sc. degree from Middle East Technical University Department of Mechanical Engineering, Ankara, in 2003. Same year, he joined Department of Mechanical Engineering at Koç University, as an M.Sc candidate. He is planning to pursue a Ph.D degree at University of Illinois at Chicago.